Dnmt3L Antagonizes DNA Methylation at Bivalent Promoters and Favors DNA Methylation at Gene Bodies in ESCs.

UNIVERSITÀ DEGLI STUDI DI TORINO

Please cite this article in press as: Neri et al., Dnmt3L Antagonizes DNA Methylation at Bivalent Promoters and Favors DNA Methylation at Gene Bodies in ESCs, Cell (2013), http://dx.doi.org/10.1016/j.cell.2013.08.056

Cell

Dnmt3L Antagonizes DNA Methylation at Bivalent Promoters and Favors DNA Methylation at Gene Bodies in ESCs

Francesco Neri,[1,4] Anna Krepelova,[1,2,4] Danny Incarnato,[1,2] Mara Maldotti,[1] Caterina Parlato,[1] Federico Galvagni,[2] Filomena Matarese,[3] Hendrik G. Stunnenberg,[3] and Salvatore Oliviero[1,2,*]

[1]Human Genetics Foundation (HuGeF), via Nizza 52, 10126 Torino, Italy

[2]Dipartimento di Biotecnologie, Chimica e Farmacia, Università degli Studi di Siena, Via Fiorentina 1, 53100 Siena, Italy

[3]Nijmegen Center for Molecular Life Sciences, Department of Molecular Biology, 6500 HB Nijmegen, The Netherlands

[4]These authors contributed equally to this work

*Correspondence: salvatore.oliviero@hugef-torino.org

http://dx.doi.org/10.1016/j.cell.2013.08.056

SUMMARY

The de novo DNA methyltransferase 3-like (Dnmt3L) is a catalytically inactive DNA methyltransferase that cooperates with Dnmt3a and Dnmt3b to methylate DNA. Dnmt3L is highly expressed in mouse embryonic stem cells (ESCs), but its function in these cells is unknown. Through genome-wide analysis of Dnmt3L knockdown in ESCs, we found that Dnmt3L is a positive regulator of methylation at the gene bodies of housekeeping genes and, more surprisingly, is also a negative regulator of methylation at promoters of bivalent genes. Dnmt3L is required for the differentiation of ESCs into primordial germ cells (PGCs) through the activation of the homeotic gene *Rhox5*. We demonstrate that Dnmt3L interacts with the Polycomb PRC2 complex in competition with the DNA methyltransferases Dnmt3a and Dnmt3b to maintain low methylation levels at the H3K27me3 regions. Thus, in ESCs, Dnmt3L counteracts the activity of de novo DNA methylases to maintain hypomethylation at promoters of bivalent developmental genes.

INTRODUCTION

In mammals, the methylation at 5mC occurs mainly at CpG dinucleotides and is required for fundamental physiological processes, such as embryonic development, X chromosome inactivation, and genomic imprinting (Okano et al., 1999; Pontier and Gribnau, 2011; Li, 2002). Genome-wide analyses and functional studies allowed researchers to correlate DNA methylation with epigenetic modifications and to identify DNA elements that are necessary for DNA methylation (Meissner et al., 2008; Hawkins et al., 2010; Lienert et al., 2011). However, the regulation of DNA methylation in stem cells and during early differentiation remains elusive.

DNA methylation is mediated by DNA methyltransferases (Dnmt), which include the maintenance enzyme Dnmt1 and the de novo Dnmt3. The family of the Dnmt3 includes two catalytically active members, Dnmt3a and Dnmt3b, and a catalytically inactive member called Dnmt3-like (Dnmt3L) (Bestor, 2000) (Jurkowska et al., 2011b).

A crystallography study showed that Dnmt3L forms a heterotetrameric complex with Dnmt3a (Jia et al., 2007). It has been suggested that this tetramerization prevents Dnmt3a oligomerization and localization in heterochromatin (Jurkowska et al., 2011a). In vitro experiments showed that Dnmt3L interacts with Dnmt3a or Dnmt3b and stimulates their activity (Chédin et al., 2002) (Chen et al., 2005; Gowher et al., 2005; Kareta et al., 2006).

In mouse embryonic stem cells (ESCs), a large number of promoters are hypomethylated. DNA methylation increases during implantation to remain stable in fully differentiated cells (Borgel et al., 2010). This methylation pattern does not correlate with Dnmt3L, which is highly expressed in ESCs, and its level drops with ESC differentiation to be re-expressed only in growing oocytes and in testes during a brief perinatal period (Bourc'his et al., 2001) (Bourc'his and Bestor, 2004). In germ cells, Dnmt3L collaborates with Dnmt3a for the methylation of imprinted loci and retrotransposons (Hata et al., 2002; Kaneda et al., 2004) (Bourc'his et al., 2001; Bourc'his and Bestor, 2004). Less clear is the role of Dnmt3L in ESCs, where Dnmt3L is highly expressed.

In ESCs, the Polycomb complex mediates the transcription repression of the genes involved in development, which is different from DNA methylation. Polycomb-mediated repression is considered to be less permanent because it maintains the possibility of activating the genes upon differentiation. It has been observed that H3K27me3-positive promoters are frequently DNA methylated during differentiation (Mohn et al., 2008) and are hypermethylated in cancer (Ohm et al., 2007; Schlesinger et al., 2007; Widschwendter et al., 2007; Simmer et al., 2012), thus showing that H3K27me3 premarks genes for DNA methylation. A direct interaction between EZH2 of the Polycomb-repressive complex 2 (PRC2) and the DNA methyltransferases Dnmt3a and Dnmt3b has been demonstrated (Rush et al.,

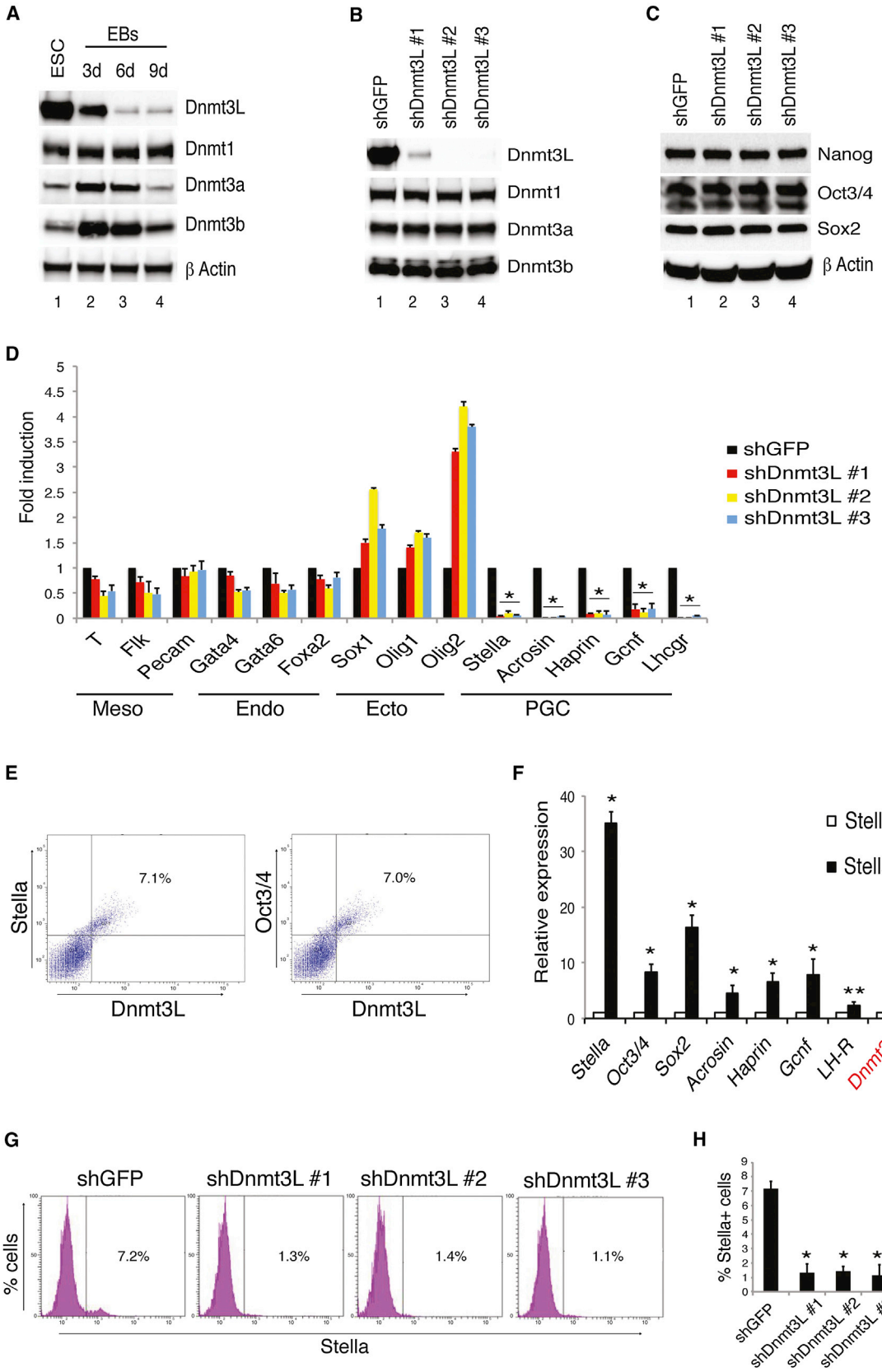

(legend on next page)

2009; Viré et al., 2006). However, a direct effect of this interaction and DNA methylation remains controversial because the binding of PRC2 is inhibited by DNA methylation in vitro (Bartke et al., 2010), and genome-wide analysis reported mutual exclusiveness of H3K27me3 with DNA methylation in CpG islands (Lindroth et al., 2008; Wu et al., 2010; Brinkman et al., 2012).

To study the role of Dnmt3L in mouse ESCs, we knocked down its expression. By genome-wide analysis, we identified differentially methylated genes and demonstrated that a fraction of these affects ESC differentiation. We found that Dnmt3L exhibits a dual role in DNA methylation because its silencing results in the reduction of the methylation in gene bodies and increased methylation at the transcription start sites of bivalent genes. Specifically, we demonstrate that Dnmt3L-dependent inhibition of DNA methylation is required for ESC differentiation into primordial germ cells (PGCs).

RESULTS

Dnmt3L Is Required for the Differentiation of Mouse ESCs into Primordial Germinal Cells

Dnmt3L is highly expressed in mouse ESCs; its expression decreases after leukemia inhibitory factor (LIF) withdrawal and remains low in embryoid bodies (EBs). In contrast, Dnmt3a and Dnmt3b levels increase following LIF withdrawal, with a peak at day 3 of EB formation, to decrease only at later time points (Figure 1A). To understand the role of Dnmt3L in ESCs, we accomplished its acute depletion by RNA interference. Three independent shRNA constructs strongly reduced Dnmt3L expression without altering the expression of Dnmt3a or Dnmt3b in ESCs (Figure 1B).

ESCs that were silenced for Dnmt3L showed minor morphological alterations and no variation in the expression of the ESC core factors Oct3/4, Nanog, and Sox2 (Figure 1C). In contrast, analysis by quantitative PCR (RT-qPCR) of embryonic markers in Dnmt3L-silenced cells after 7 days of ESC differentiation into EBs showed an unbalanced expression of the markers of the three embryonic germ layers and of the primordial germ cells (PGC) (Figure 1D). Importantly, the markers of PGC, Stella (indicated as Dppa3), Acrosin, Haprin, Gcnf, and LH-R were almost undetectable (Figure 1D), which suggests that Dnmt3L is involved in PGC establishment.

Next, we analyzed whether Dnmt3L is actually expressed in PGC cells (Stella positive) in EBs at 7 days. Fluorescence-activated cell sorting (FACS) analysis of EBs showed that Stella-positive PGC cells, which maintain the expression of Oct3/4 (Wei et al., 2008), were also positive for Dnmt3L (Figure 1E and Figure S1). The coexpression of Stella with Dnmt3L was confirmed by immunofluorescence on ESCs that were differentiated in a monolayer (Figure S1A). Dnmt3L mRNA was significantly enriched together with other known markers of PGCs, including Sox2, Acrosin, Haprin, Gcnf, and LH-R, in Stella-positive versus Stella-negative sorted cells from 7-day EBs (Figure 1F). Moreover, by FACS analysis, we observed a reduction of ~85% of the Stella-positive PGCs by Dnmt3L silencing (Figures 1G and H). To verify that the phenotype observed was not due to silencing-dependent off-target effects, we also performed the knockout of Dnmt3L by targeting the first exon of Dnmt3L using the transcription activator-like effector nucleases (TALENs) (Boch et al., 2009; Moscou and Bogdanove, 2009) (Figures S1D–S1F). Phenotypic analysis of two independent Dnmt3L knockout ESC clones showed, similarly to the phenotype observed with knockdown experiments, the impairment of PGC markers (compare Figures S1H and S1I with Figures 1D and 1E).

These experiments establish that Dnmt3L is an early marker of PGCs and that its expression is required for ESC differentiation toward PGCs.

Dnmt3L Modulates the Expression of the *Rhox* Genes, which Are Required for ESC-to-PGC Differentiation

To identify the genes that are regulated by the Dnmt3L, we performed microarray analysis of the three shRNAs (Pearson correlation $R \geq 0.87$, Figure S2A). The microarray analysis of the control and Dnmt3L knockdown ESCs identified 777 upregulated and 467 downregulated genes (Table S1). To identify among the Dnmt3L-regulated genes those that were involved in ESC differentiation into PGCs, we compared this list of Dnmt3L-regulated genes with the genes that are differentially expressed in PGC (Stella-positive) versus non-PGC (Stella-negative) EBs, which were previously published (West et al., 2009). This analysis identified 60 genes that are upregulated by Dnmt3L knockdown and that were also upregulated in Stella-negative cells and 67 genes that were downregulated in Dnmt3L

Figure 1. Dnmt3L Is a Marker of Primordial Germinal Cells, and Its Knockdown Alters Correct PGCs Formation

(A) Dnmt3L is highly expressed in ESCs and strongly decreases during EBs development, which is different from the other Dnmts. Protein levels were measured by western blot analysis, as indicated. β-actin was used as a loading control.

(B) Knockdown of Dnmt3L performed with three different shRNAs in ESCs efficiently decreased the Dnmt3L protein level, though it did not alter the level of the other Dnmts. The protein levels were measured by western blot analysis, as indicated.

(C) Knockdown of Dnmt3L performed as in (B) did not alter the expression of pluripotency-related genes, such as Nanog, Oct3/4, and Sox2. The protein levels were measured by western blot analysis. β-actin was used as a loading control.

(D) RT-PCR analysis shows a significant reduction in the PGC markers, such as Stella (Dppa3), Acrosin, Haprin, Gcnf, and LH-R in Dnmt3L knockdown ESCs differentiated in EBs for 7 days, and no significant differences were noted in the markers of the other germinal layers. *$p < 0.001$. Data are represented as mean ± SD.

(E) FACS analysis demonstrates that Dnmt3L is expressed together with Stella and Oct3/4 in the PGCs of differentiated EBs.

(F) RT-PCR analysis of Stella-positive cells sorted out of the EBs on the seventh day shows a significant enrichment of Dnmt3L mRNA in Stella-positive cells with respect to Stella-negative cells (*$p < 0.001$, **$p < 0.05$). Data are represented as mean ± SD.

(G) Knockdown of Dnmt3L led to an almost 80% reduction in the Stella-positive cells in differentiated EBs, as shown by the FACS analysis.

(H) Quantification of Stella-positive cells in the FACS experiment shown in (G) (*$p < 0.001$). Data are represented as mean ± SD.

See also Figure S1.

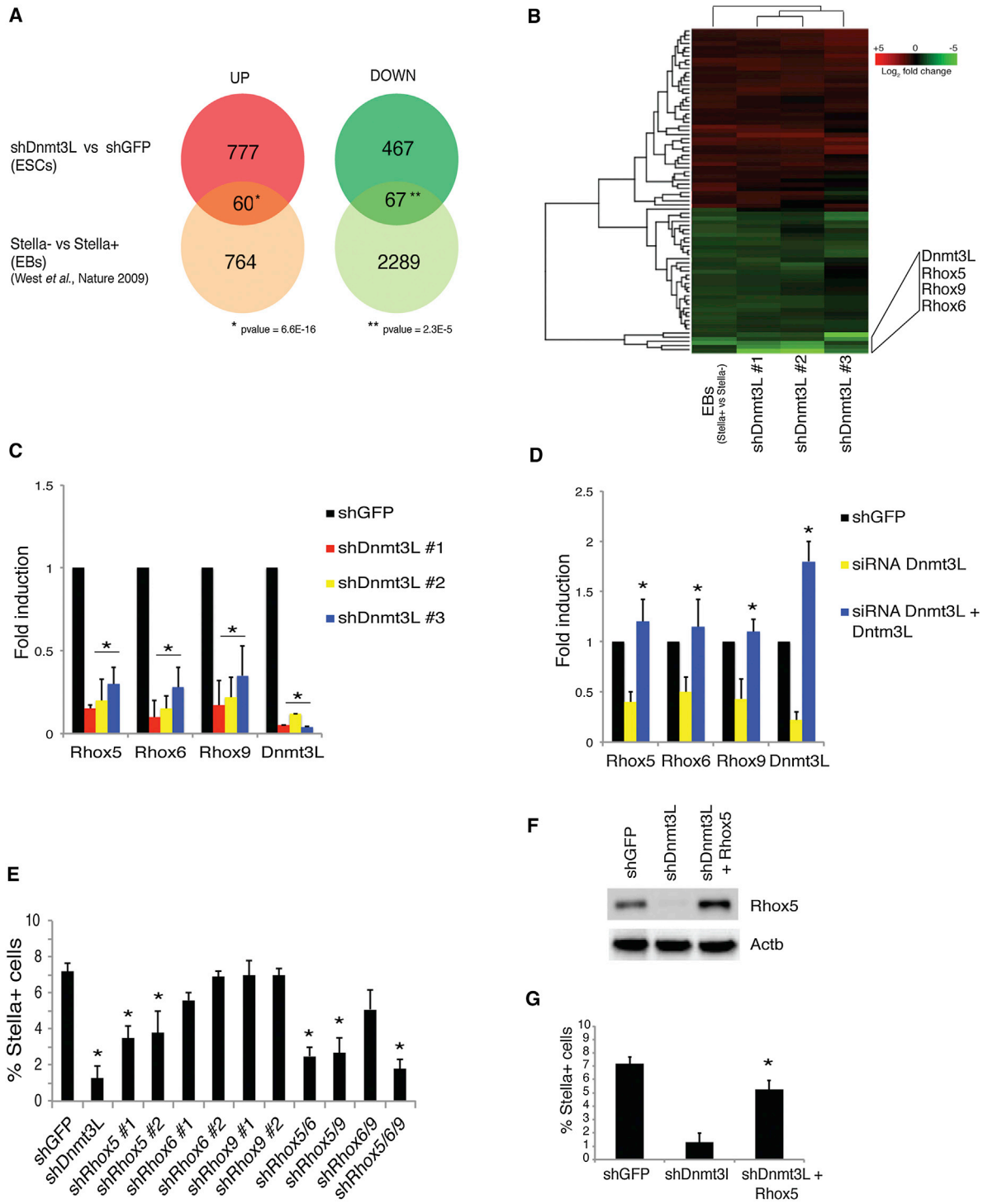

Figure 2. Dnmt3L Modulates the Expression of the *Rhox* Family Genes to Control the PGC Correct Development

(A) A comparison of the genes that are regulated upon Dnmt3L knockdown against the genes that are differentially expressed in PGCs (Stella +) versus non-PGCs (Stella−) of differentiated EBs.

(B) The heatmap of the shared genes shown in (A). The *Rhox5*, *Rhox6*, and *Rhox9* genes are the most downregulated genes of those that are clustered with Dnmt3L.

(C) The downregulation of the three *Rhox* genes upon Dnmt3L knockdown was confirmed by RT-PCR analysis (*$p < 0.001$). Data are represented as mean ± SD.

(D) RT-PCR analysis of the *Rhox* genes upon Dnmt3L rescue. The endogenous Dnmt3L was silenced by a siRNA targeting the 3′UTR (*$p < 0.001$). Data are represented as mean ± SD.

(legend continued on next page)

knockdown and were also downregulated in Stella-negative cells (Figures 2A and 2B). Cluster analysis revealed that Dnmt3L was coregulated with three members of the *Rhox* (reproductive homeobox on X-chromosome) family: *Rhox5*, *Rhox6*, and *Rhox9* (Figure 2B). Further comparison of Dnmt3L-regulated genes versus mouse-derived PGCs and other tissue-regulated genes (Hayashi et al., 2011; Shen et al., 2008; Turbendian et al., 2013) confirmed the coregulation of Dnmt3L with *Rhox* genes (Figures S2C and S2D).

Because *Rhox* genes encode for transcription factors that are regulated by DNA methylation (Maclean et al., 2011) and their expression is crucial for differentiation of ES cells (MacLean and Wilkinson, 2010), we further analyzed the expression of the *Rhox* genes in Dnmt3L knockdown cells. The downregulation of the three *Rhox* genes upon Dnmt3L silencing was confirmed by RT-qPCR (Figure 2C). The specificity of Dnmt3L-dependent regulation was further verified by a complementation assay in which the silencing of the endogenous gene with a siRNA that targets the 3′UTR was rescued by the expression of an exogenous Dnmt3L (Figure 2D). Furthermore, we observed the downregulation of *Rhox* genes in *Dnmt3L*$^{-/-}$ ESCs (Figure S2E). Next, we verified whether the knockdown of the *Rhox* genes could affect the differentiation of ESCs into PGCs. We compared the efficiency of ESC differentiation into PGCs by expressing shRNA for Rhox5, Rhox6, Rhox9, or combinations of these constructs by measuring the number of Stella-positive cells in EBs on day 7. The silencing of *Rhox5*, either alone or in combination with *Rhox6* and/or *Rhox9*, induced a significant reduction of Stella-positive cells in EBs, whereas the silencing of *Rhox6* and *Rhox9* did not show a significant reduction in the Stella-positive cells (Figures 2E and S2F). To establish whether Dnmt3L knockdown prevents PGC formation by repressing *Rhox5*, we expressed *Rhox5* in Dnmt3L-silenced cells (Figure 2F). Analysis of Stella-positive cells showed that *Rhox5* ectopic expression rescues the block of PGC differentiation following Dnmt3L silencing (Figure 2G). Thus, Dnmt3L is required for the differentiation of PGCs via the regulation of *Rhox5*.

Dnmt3L Maintains *Rhox5* Gene Expression by Inhibiting DNA Methylation on the *Rhox5* Promoter Region

We next analyzed the pattern of *Rhox5* methylation in wild-type and Dnmt3L knockdown ES cells. The *Rhox5* gene is transcribed from two alternative promoters: a distal promoter (Pd) and a proximal promoter (Pp) (Figure 3A), which transcribe two mRNAs that differ in their 5′ untranslated regions. In ESCs, only the distal promoter is active (Li et al., 2011) (Figures S2G and S2H).

Because Dnmt3L has been shown to cooperate with Dntm3a and Dnmt3b to methylate the DNA and because *Rhox* genes are upregulated in Dntm3a/3b ESC double knockouts (DKOs) (Figure S2G) (Maclean et al., 2011), we expected that the Dnmt3L knockdown would result in *Rhox5* downmethylation. Instead, bisulfite sequencing and methylated DNA immunoprecipitation (MeDIP) of the *Rhox5* promoter region revealed that Dnmt3L knockdown induces a significant increase in DNA methylation at both the distal and proximal promoters (Figures 3A and 3B). Dnmt3L silencing also affected DNaseI accessibility and increased the level of the repressive mark H3K9me3 within this region (Figures 3C and S2I). ChIP experiments revealed that Dnmt3L associates with the *Rhox5* promoter region, and its signal was significantly reduced by Dnmt3L knockdown (Figure 3D). In contrast, Dnmt3a and Dnmt3b showed a low association with the *Rhox5* promoter region in wild-type ESCs, and their binding increased significantly upon Dnmt3L knockdown (Figures 3E and 3F). To measure the dynamics of Dnmt3L-dependent regulation of *Rhox5* we generated Dnmt3L-ER-*Dnmt3L*$^{-/-}$ stable clones. Time-course analysis of 4-hydroxitamoxifen (OHT) withdrawal, which leads to the cytoplasmic localization of the Dnmt3L-ER fusion protein, showed a concomitant reduction of the *Rhox5* expression and an increase of its DNA methylation, together with a reduction of its accessibility (Figures S2J–S2M).

The Dual Functions of Dnmt3L in DNA Methylation

The above results demonstrate that Dnmt3L inhibits methylation at the *Rhox5* promoter region and suggest that, in this region, Dnmt3L acts as a competitor of Dnmt3a and Dnmt3b. This result is surprising considering that Dnmt3L has been previously reported to cooperate in vitro with Dnmt3a and Dnmt3b to methylate the DNA (Suetake et al., 2004; Chen et al., 2005). To verify whether the Dnmt3L-dependent inhibition of DNA methylation is a general feature, we performed genome-wide methylation analysis by MeDIP-seq in control and Dnmt3L-silenced cells. The level of 5mC in the control cells along the entire genome, including the gene promoters, and the intragenic and intergenic regions was comparable to other MeDIP-seq analyses (Matarese et al., 2011; Ficz et al., 2011; Pastor et al., 2011) (Figures S3A and S3B). Dnmt3L silencing resulted in a reduction in the methylation at 14,107 genomic regions (Figure 4A). This result is in agreement with the Dnmt3L function of cooperating with Dnmt3a and Dnmt3b to accomplish DNA methylation. However, Dnmt3L silencing also induced a significant increase in methylation in 5,724 genomic regions (Figure 4A), which suggests that Dnmt3L also plays a role in limiting the DNA methylation. The reduction in methylation occurred mainly within the gene bodies, whereas the increase in methylation was more centered at the transcription start site (TSS) (Figure 4B). Analysis of the methylation distribution was performed by using a list of the genes that was ordered with respect to the level of their

(E) Quantification of FACS analysis of Stella-positive cells in PGCs upon knockdown of *Rhox* genes in ESCs (*$p < 0.01$). The efficiency of PGC differentiation of ESCs that express the shRNA for *Rhox5*, *Rhox6*, *Rhox9*, or combinations of these constructs was measured as the number of Stella-positive cells in EBs on day 7. The silencing of *Rhox5* either alone or in combination with *Rhox6* and/or *Rhox9* induced a significant reduction in the Stella-positive cells in EBs, whereas the silencing of *Rhox6* and *Rhox9* did not show a significant reduction in the Stella-positive cells. Data are represented as mean ± SD.

(F) Western blot analysis of the total extracts obtained from the control, Dnmt3L knockdown, and Dnmt3L knockdown cells that overexpress exogenous *Rhox5*. β-actin was used as a loading control.

(G) Quantification of FACS analysis of Stella-positive cells upon Dnmt3L knockdown and *Rhox5* rescue (*$p < 0.001$). Data are represented as mean ± SD.

See also Figure S2 and Tables S1 and S2.

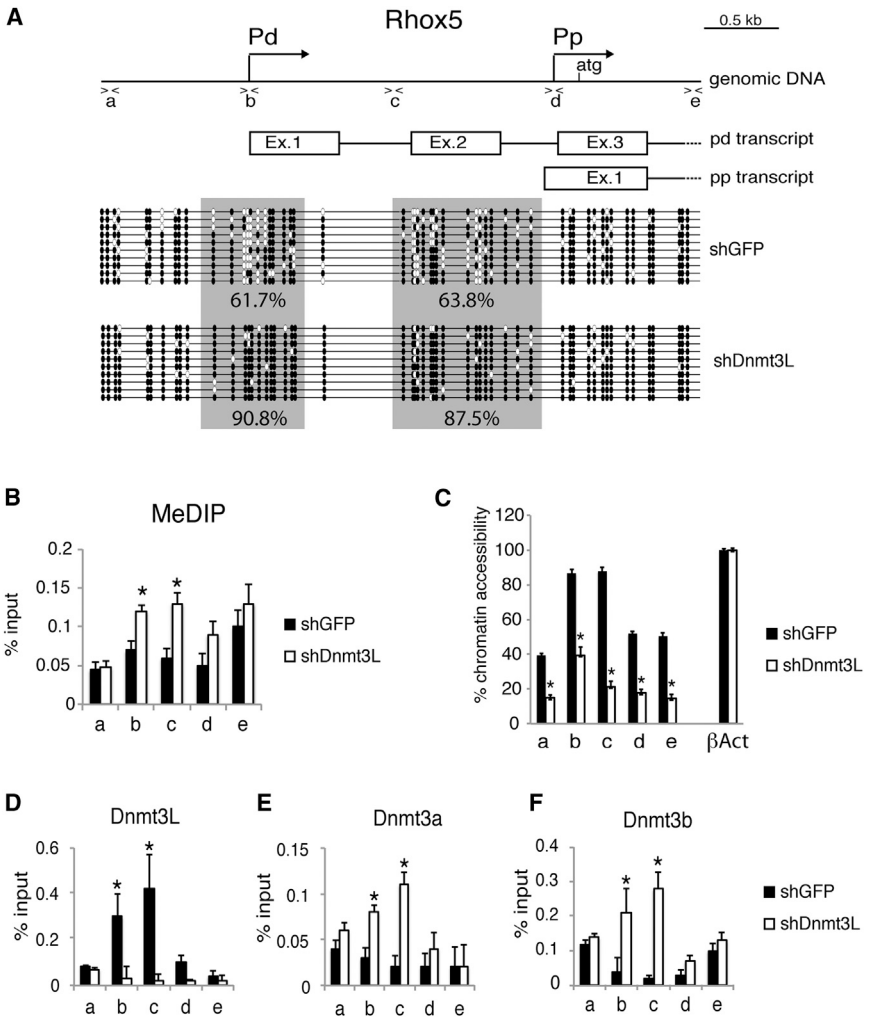

Figure 3. Dnmt3L Maintains the *Rhox5* Gene in an ON State by Inhibiting Its DNA Methylation at Its Promoter

(A) Bisulfite analysis within the *Rhox5* promoter region shows a significant increase of DNA methylation at the distal promoter (Pd) and at the second exon (Ex.2) upon Dnmt3L knockdown. Pd, distal promoter; Pp, proximal promoter. Lowercase letters show the position of the primers for the ChIP analysis.

(B) MeDIP analysis shows a significant increase in DNA methylation at the distal promoter and at the level of the second exon (Ex.2) upon Dnmt3L knockdown

*$p < 0.01$. Data are represented as mean ± SD.

(C) A reduction in the DNaseI sensitivity (measured as a percentage of chromatin accessibility) is observed within the shown *Rhox5* regions upon Dnmt3L knockdown. *$p < 0.001$. The β-actin gene was used as a control. Data are represented as mean ± SD.

(D–F) ChIP analysis of Dnmt3L, Dnmt3a, and Dnmt3b binding to the *Rhox5* regions. Dnmt3L associates with the *Rhox5* promoter region, and its signal is significantly reduced upon Dnmt3L knockdown, whereas Dnmt3a and Dnmt3b show a low association with the *Rhox5* promoter region in wild-type ESCs, and their binding increases significantly upon Dnmt3L knockdown. *$p < 0.001$. Data are represented as mean ± SD.

See also Figure S2.

expression; this analysis showed a significant increase in methylation at the promoters of genes that were not expressed or were expressed at a low level (Figures 4C and S3C). Gene ontology analysis showed that the genes that had increased methylation were significantly enriched for developmental genes, most of which are bivalent in ESCs (Figures S3D and S3E). The reduction in methylation was centered more on the body of genes that had higher expression levels and included genes that are involved in cell growth and metabolism (Figures 4C and S3E).

To explore the relation between histone modifications and the Dnmt3L-dependent DNA methylation, we compared the increase in DNA methylation that resulted from Dnmt3L silencing with respect to histone modifications. Dnmt3L-dependent methylation (Figure 4D, loss of 5mC) showed a 9% overlap with the bodies of the H3K4me3 genes over a total of 7,931 ($p < 10^{-7}$), which is in agreement with a role for Dnmt3L in cooperating with Dnmt3a and Dnmt3b to methylate DNA. Importantly, we also found that the increase in DNA methylation correlates with bivalent genes because 55% of the H3K27me3/H3K4me3-positive genes over a total of 2,189 genes ($p = 0.00$) showed an increase in DNA methylation following Dnmt3L silencing (Figure 4D, gain of 5mC). Remarkably, Dnmt3L silencing induced an increase of 5mC in the H3K27me3-positive regions (Figure 4E). Interestingly, the analysis of the gain of methylation on the H3K27me3 promoters classified by the level of DNA methylation resulted to be independent of their initial methylation state and correlates with the increase of DNA methylation that is observed during ESC differentiation (Stadler et al., 2011) (Figures S3F and S3G). The gain in 5mC was validated by the bisulfite technique (Figure S4). These results establish that one role of Dnmt3L in ESCs is to maintain the hypomethylated state of the bivalent genes.

Dnmt3L Forms a Complex with PRC2 via its Direct Interaction with Ezh2

The above results show that, in ESCs, the increase in DNA methylation by Dnmt3L silencing overlaps with H3K27me3 modification. In differentiated cells, the Polycomb PRC2 complex associates with Dnmt3a and Dnmt3b (Viré et al., 2006). However, in ESCs, the majority of H3K27me3 genes are hypomethylated (Fouse et al., 2008; Rush et al., 2009), which suggests that a more complex interplay between PRC2 and DNA methyltransferases takes place in ESCs.

By using coimmunoprecipitation of endogenous proteins, we tested whether the PRC2 complex could interact with Dnmt3L.

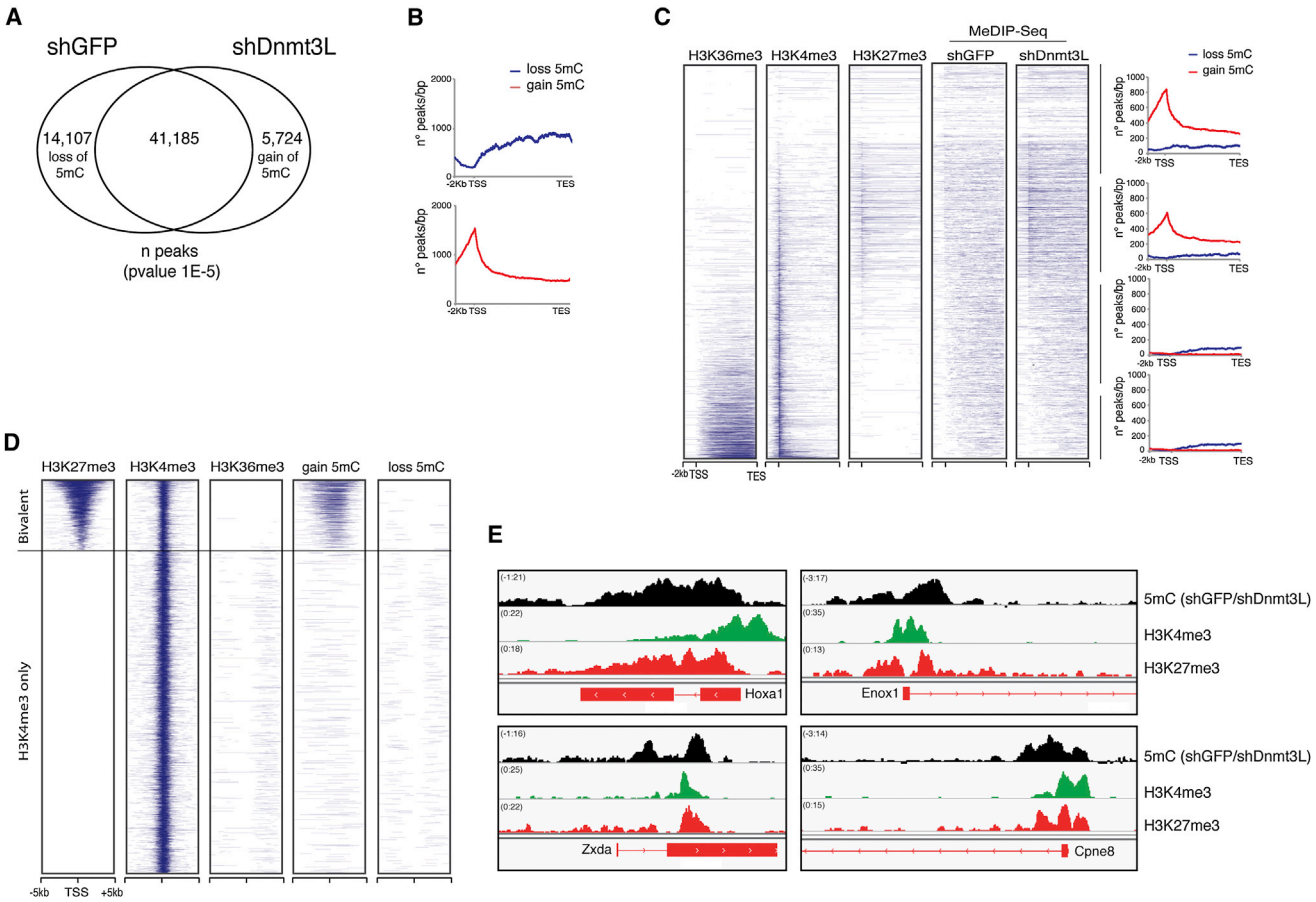

Figure 4. The Double Role of Dnmt3L in 5mC Regulation

(A) Venn diagram showing the DNA methylated regions in the control and/or the Dnmt3L knockdown cells. Dnmt3L silencing results in a reduction in the methylation in 14,107 genomic regions as well as in an increase in the methylation in 5,724 genomic regions.

(B) Loss of methylation occurs mainly within gene bodies, whereas a gain of methylation occurs at the TSS of the gene promoters.

(C) Heatmap representations of genomic regions marked by H3K36me3, H3K4me3, and H3K27me3 modifications and by 5mC in control and Dnmt3L knockdown cells. The heatmap is rank ordered from the less-expressed (top) to the most-expressed (bottom) genes. Analysis of the methylation distribution shows an increase in methylation at the gene promoters of nonexpressed or low-expressed genes.

(D) Heatmap representations of genomic regions ordered by the H3K27me3 level at gene promoters. The regions that show a gain in the DNA methylation upon Dnmt3L knockdown positively correlate with H3K27me3 modification.

(E) Example of four bivalent genes that become methylated upon Dnmt3L knockdown. The difference between the 5mC genomic occupancy of the control and Dnmt3L knockdown cells (in black) are shown, together with associated histone modification patterns.

See also Figures S3 and S4.

We observed that, in ESCs, in addition to Dnmt3a and Dnmt3b, Dntm3L also coimmunoprecipitated with Ezh2 and Suz12 (Figure 5A), and in the reciprocal experiment, both proteins of the PRC2 complex coimmunoprecipitated with Dnmt3L (Figure S5A). We further demonstrated through an in vitro interaction assay using the recombinant FLAG-Dnmt3L and GST-Ezh2 proteins that the observed interaction is direct (Figures 5B and S5B). Moreover, by increasing salt concentrations, we observed a higher affinity of Ezh2 with Dnmt3L with respect to Dnmt3a/b (Figures S5B and S5C). By deletion mutants, we mapped the interaction of Dnmt3L with Ezh2 to the Dnmt3L N-terminal part, within its PHD like domain; in agreement with previous reports (Suetake et al., 2004), the deletion of the C-terminal domain abolished its interaction with Dnmt3a (Figure 5C).

Furthermore, we fractionated the nuclear protein complexes through gel filtration chromatography and immunoprecipitated each fraction with anti-Dnmt3L antibody. Western blot analysis revealed that the Dnmt3L protein immunoprecipitated different complexes containing Ezh2, Dnmt3a, or Dnmt3b at different molecular weights (Figure 5D).

Dnmt3L Competes with Dnmt3a and Dnmt3b for Binding with PRC2

The above results suggest that Dnmt3L forms a complex with PRC2 that is independent from Dnmt3a or Dnmt3b. To verify this hypothesis, we first coimmunoprecipitated Dnmt3L with Ezh2 in Dnmt3a/3b DKO ESCs and still observed the reciprocal interaction (Figure 6A). Then, we immunodepleted both Dnmt3a

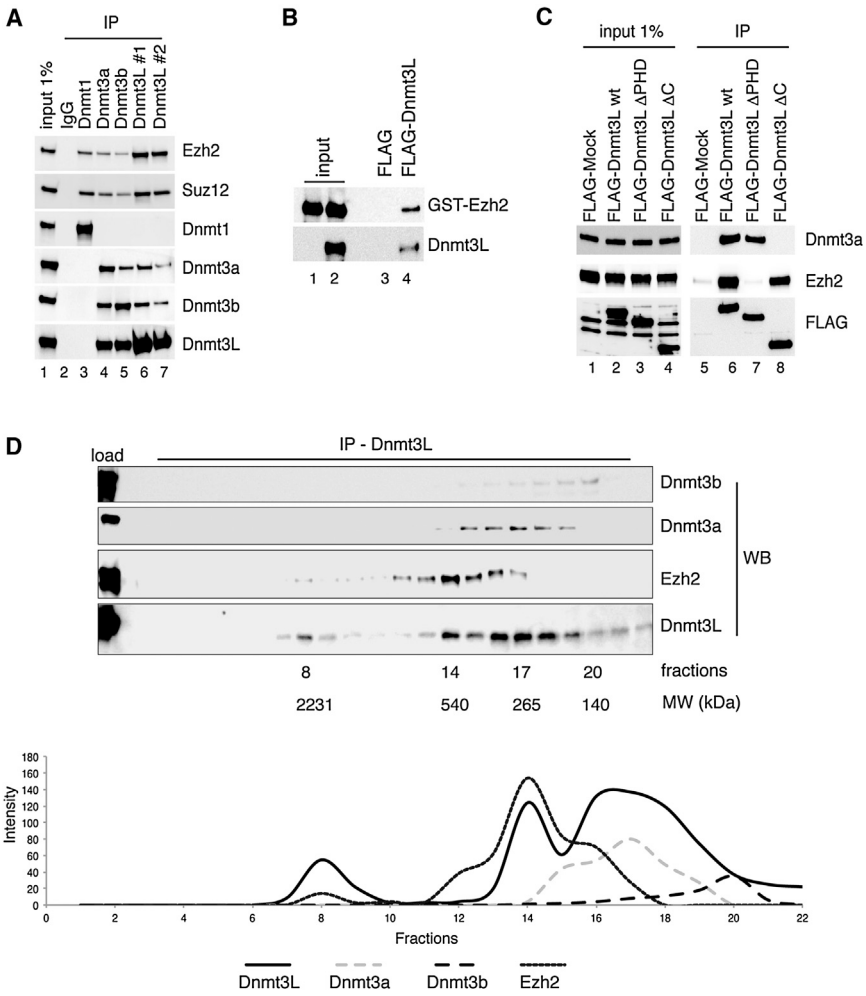

Figure 5. Dnmt3L Interacts with PRC2 through Its Direct Binding to Ezh2

(A) Endogenous Dntm3L interacts with PRC2 proteins Ezh2 and Suz12 in ESCs, as shown by immunoprecipitation. Two different antibodies against Dnmt3L were used. 1% of the nuclear extract was loaded as an input.

(B) In vitro interaction assay with recombinant GST-Ezh2 and FLAG-Dnmt3L proteins demonstrates a direct interaction between the two proteins.

(C) The PHD-like domain of Dnmt3L is responsible for the direct interaction with the Ezh2 protein, as demonstrated by deletion mutant analysis. The ESCs were transiently transfected with the indicated FLAG-tagged deletion mutants, and the proteins were immunoprecipitated by anti-FLAG M2 magnetic beads. The interacting proteins were analyzed by immunoblotting using the indicated antibodies. One percent of the nuclear extract was loaded as an input.

(D) Gel filtration analysis of Dnmt3L protein complexes. ESC nuclear extract was separated on Superose-6 10/300 GL column and immunoprecipitated with anti-Dnmt3L antibody followed by immunoblotting with the indicated antibodies to reveal the different complexes. The bottom panel shows the quantification.

See also Figure S5.

and Dnmt3b from the nuclear extracts of wild-type ESCs to remove all Dnmt3a- and Dnmt3b-associated complexes. The immunodepleted extracts still coimmunoprecipitated Dnmt3L with Ezh2 but no longer coimmunoprecipitated Dnmt3a or Dnmt3b with Ezh2 (Figure S6A). Finally, we performed a double immunoprecipitation of transfected FLAG-Dnmt3L. The first immunoprecipitation performed with the anti-FLAG antibody coimmunoprecipitated Ezh2 as well as the Dnmt3a and Dnmt3b proteins (Figure 6B, lane 1). Then, we performed re-immunoprecipitations using antibodies against the endogenous proteins of interest. We observed that Dnmt3L forms a different complex with Ezh2 compared with the complex that it forms with Dnmt3a/3b (Figure 6B, lanes 3–5). Taken together, the above experiments establish that, in ESCs, Dnmt3L interacts directly with PRC2 in a complex that is independent from those formed by PRC2 with Dnmt3a or Dnmt3b.

Because the ChIP experiments showed increased binding of Dnmt3a and Dnmt3b on the *Rhox5* gene in Dnmt3L-silenced cells (Figures 3E and 3F), we further verified whether Dnmt3L could compete with Dnmt3a or Dnmt3b for the interaction with the PRC2 complex.

We observed that there was an increase of the Ezh2 coimmunoprecipitate with Dnmt3a and Dnmt3b in extracts from Dnmt3L-silenced cells, compared with the extracts from control cells (Figure 6C, top) as well as a significant increase of the DNA methylation activity of the immunoprecipitated fractions (Figures 6C, bottom and S6B). To further demonstrate the competition between Dnmt3L and Dnmt3a/3b for the interaction with the PRC2 complex, we analyzed the immunoprecipitate of Ezh2 with Dnmt3 proteins in HEK293 cells, which do not express Dnmt3L, by expressing in these cells a FLAG-tagged Dnmt3L under an inducible promoter. Increasing the concentration of FLAG-Dnmt3L completely abolished the coimmunoprecipitation of Ezh2 with Dnmt3a and Dnmt3b (Figure 6D). These experiments demonstrate that Dnmt3L is a direct competitor of Dnmt3a and Dnmt3b for the interaction with PRC2.

Dnmt3L Is Recruited by PRC2 at H3K27me3 Genes

Because *Rhox5* is a bivalent gene that is marked by H3K27me3 and is bound by Ezh2 (Figure S7A) (Li et al., 2011), we further analyzed the interplay between Dnmt3L and PRC2 on its promoter region (Figure 7A). Suz12 silencing resulted in a significant reduction of PRC2 binding to the *Rhox5* promoter region, as measured by the chromatin immunoprecipitation (ChIP) of Ezh2 (Figures 7B and 7C), together with a reduction in H3K27me3 (Figure S7B). Importantly, the reduction of PRC2 association with *Rhox5* significantly affected the Dnmt3L binding to this region (Figure 7D), which demonstrates that Dnmt3L is recruited by PRC2 on *Rhox5*.

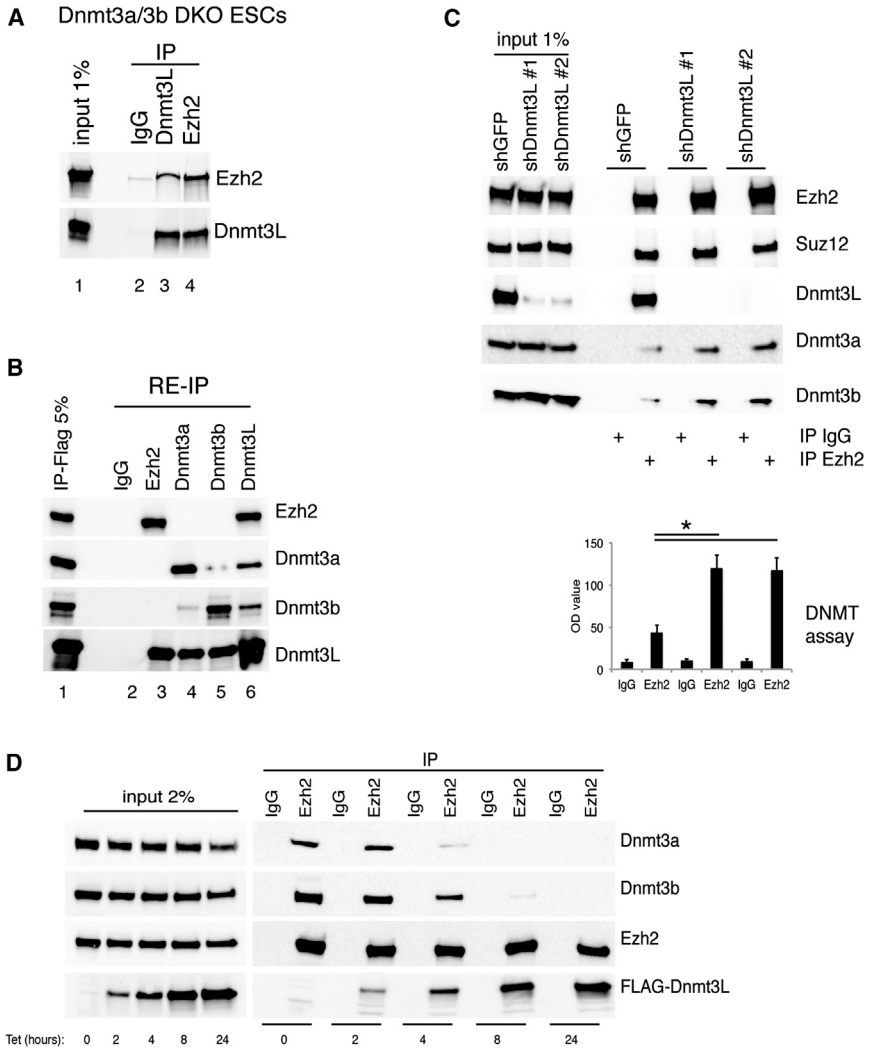

Figure 6. Dnmt3L Competes with Dnmt3a/3b for PRC2 Binding in ESCs

(A) Dnmt3L coimmunoprecipitates with Ezh2 protein also in Dnmt3a/b dKO ESCs. The endogenous proteins were immunoprecipitated using the indicated antibodies. One percent of the nuclear extract was loaded as an input.

(B) Re-immunoprecipitation analysis demonstrates that Dnmt3L together with Ezh2 occur in a protein complex that does not contain Dnmt3a/3b proteins. The ESCs were transiently transfected with FLAG-Dnmt3L, and the first immunoprecipitation was performed using the anti-FLAG antibody. The interacting proteins were eluted with FLAG peptide and were subsequently re-immunoprecipitated using the indicated antibodies.

(C) Dnmt3L knockdown in ESCs leads to an increase in the interaction between the Ezh2 and Dnmt3a/3b proteins and, in addition, leads to a corresponding increase in the DNA methylation activity of the immunoprecipitates (bottom). The immunoprecipitation experiments were performed using two different shRNAs for Dnmt3L. *$p < 0.001$. Data are represented as mean ± SD.

(D) Competition analysis in HEK293 cells that stably express the FLAG-Dnmt3L protein. The induction of FLAG-Dnmt3L protein by the tetracycline treatment for the indicated times leads to a loss in the interaction between the Ezh2 and Dnmt3a/3b proteins, as shown by immunoprecipitation.

See also Figure S6.

To verify whether Dnmt3L is recruited to the chromatin via PRC2 genome wide, we performed ChIP-seq analysis of Bio-Dnmt3L in control or Suz12-silenced ESCs (Figure 7E). As expected, we observed that Bio-Dnmt3L was localized on gene bodies of transcriptionally active genes involved in cell metabolism and on the H3K27me3-positive promoters of developmental genes (Figures 7F–7I and S7C–S7E). Analysis of Bio-Dnmt3L distribution on genes ordered by the level of H3K27me3 showed a significant reduction of Bio-Dnmt3L binding specifically at the H3K27me3 promoters, but not on the H3K27me3-negative genes (Figures 7J and 7K), as is evident from the representative cluster of the Hoxa genes (Figure 7L). In contrast, the silencing of Dnmt3L did not alter the genomic distribution of PRC2 measured by ChIP-seq of Suz12 (Figure S7F–S7I).

DISCUSSION

Although it has been demonstrated that there is a correlation between certain epigenetic marks and DNA methylation (Meissner et al., 2008), the mechanism that regulates its specificity has not yet been clarified. Here, we have shown that, in ESCs, the noncatalytic member of the de novo DNA methyltransferases Dnmt3L plays a regulatory role on the DNA methylation by enhancing or inhibiting the activity of Dnmt3a and Dnmt3b in different chromatin contexts. Specifically, Dnmt3L enhances the DNA methylation at gene bodies of active genes and prevents DNA methylation at the promoters of H3K27me3-positive genes.

We observed that, in ESCs, Dnmt3L interacts with Dnmt3a and Dnmt3b, suggesting that Dnmt3L could stimulate their activity and/or their redistribution. This result is in agreement with the previous observation that Dnmt3L enhances in vitro the methylation activity of Dnmt3a and Dnmt3b (Suetake et al., 2004) and mediates the release of Dnmt3a from heterochromatic to euchromatic regions (Jurkowska et al., 2011a).

In ESCs, the repression of developmental genes is mediated by the Polycomb complex, which provides a reversible repression that ensures their dynamic regulation either by gene activation or by DNA methylation during differentiation (Boyer et al., 2006; Lee et al., 2006; Mohn et al., 2008; Schuettengruber and Cavalli, 2009).

Our genome-wide analysis shows that Dnmt3L, recruited by PRC2 on the H3K27me3 promoters, inhibits the methylation of the DNA at such promoters, suggesting that Dnmt3L cooperates

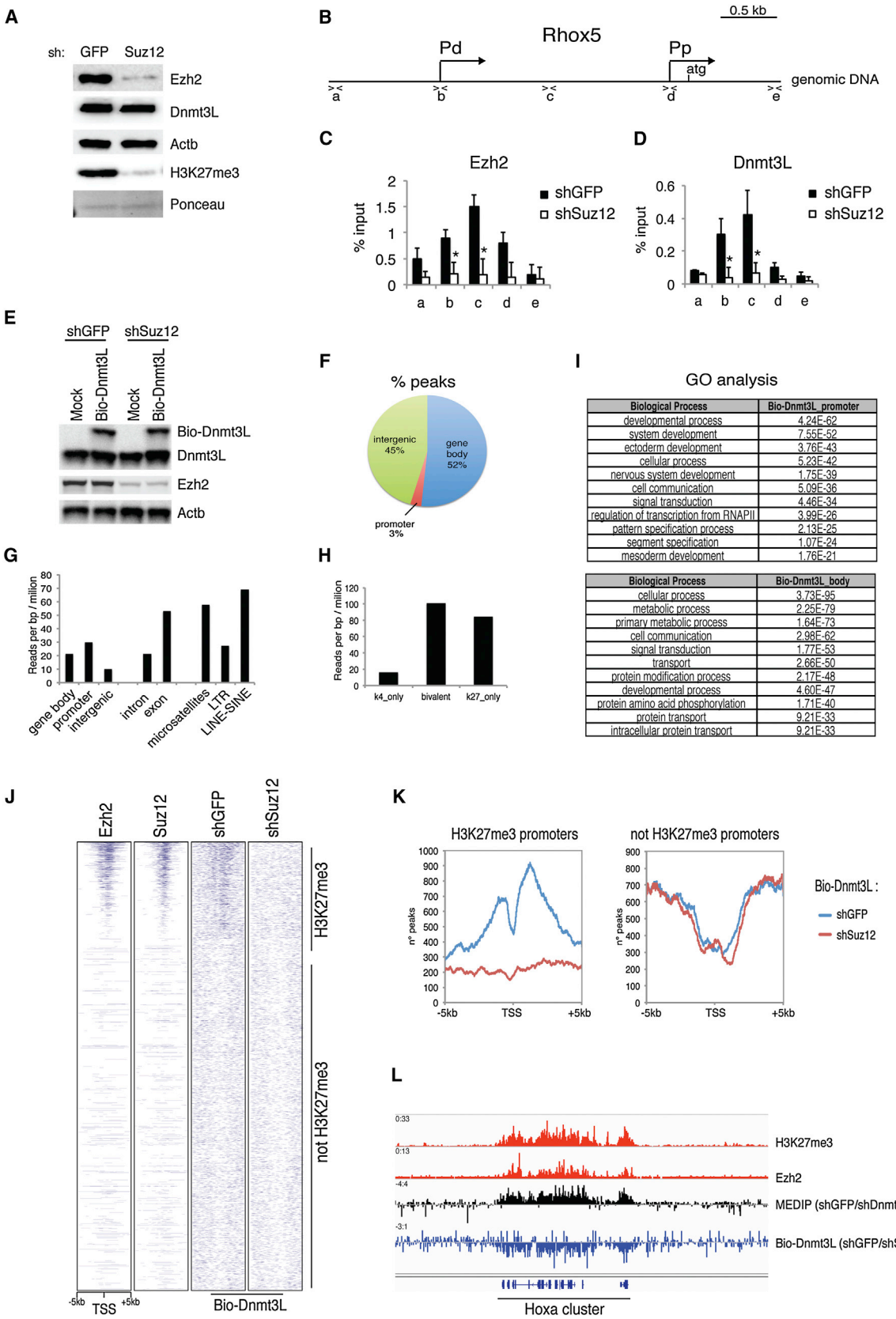

(legend on next page)

with Polycomb to keep developmental genes able to be activated upon differentiation.

It was previously shown that PRC2 is not required for ESC self-renewal but that ESCs that are defective in their PRC2 function show misregulation in their developmental programs (Pasini et al., 2007; Margueron and Reinberg, 2011). Similarly, Dnmt3L-dependent modulation of DNA methylation is not required for ESC maintenance, but it is necessary for the correct differentiation of ESCs. Previous studies have established that Dnmt3L is required in germ cells for the methylation of DNA of imprinted genes (Hata et al., 2002; Kaneda et al., 2004; Bourc'his et al., 2001). We have now observed that Dnmt3L also plays a role in ESC commitment because Dnmt3L knockdown showed unbalanced differentiation and failure to form PGCs. We found that the expression of the homeotic gene *Rhox5* depends on Dnmt3L in ESCs, and we demonstrated that *Rhox5* expression is required for ESC differentiation into PGCs. In the absence of Dnmt3L, Dnmt3a and Dnmt3b significantly increase their association to the *Rhox5* promoter region, which becomes heavily DNA methylated, leading to gene repression. PRC2 is the key player of this regulation because we demonstrated that Dnmt3L interacts directly with Ezh2 of the PRC2 complex and that Dnmt3L is recruited to the *Rhox5* promoter region via PRC2 through its PHD-like domain in competition with Dnmt3a and Dnmt3b. Thus, on the *Rhox5* promoter region, Dnmt3L binding via PRC2 inhibits the recruitment of Dnmt3a and Dnmt3b, which keeps the region hypomethylated.

Interestingly, the PHD-like domain is conserved in all three Dnmts, and it has been previously demonstrated to be instrumental for the recruitment of these methylases to the unmethylated H3K4 (Zhang et al., 2010; Ooi et al., 2007), which is not present on promoters of active and bivalent genes. We have now described a new regulatory function of the PHD-like domain that mediates the competition of Dnmt3L with Dnmt3a and Dnmt3b. We propose a model in which Dnmt3L, recruited to the chromatin at the Polycomb target genes, inhibits the recruitment of the active DNA methyltransferases Dnmt3a and Dnmt3b, in this way inhibiting the methylation at the H3K27me3-positive regions. Upon ESC differentiation, the downregulation of Dnmt3L permits de novo DNA methylation on the sites that maintain H3K27me3 modification and transcriptional activation of the genes that lose this chromatin mark.

EXPERIMENTAL PROCEDURES

Cell Culture and Differentiation Conditions

Mouse ESCs were cultured in DMEM high-glucose medium (Invitrogen) supplemented with 15% FBS (Millipore), 0.1 mM nonessential amino acids (Invitrogen), 1 mM sodium pyruvate (Invitrogen), 0.1 mM 2-mercaptoethanol, 1,500 U/ml LIF (Millipore), 25 U of penicillin/ml, and 25 μg of streptomycin/ml.

Culture and differentiation of E14 mouse ESCs into EBs has been described previously (Neri et al., 2012). For monolayer differentiation, 3×10^5 cells per well were plated on collagen IV (Col. IV)-coated 6-well dishes (Becton Dickinson) in differentiation medium (α-MEM with 15% FCS and 50μM 2-mercaptoethanol).

The T-Rex 293 cell line was cultured in DMEM high-glucose medium (Invitrogen) supplemented with 10% fetal bovine serum (FBS) (Sigma), 1 mM sodium pyruvate (Invitrogen), 50 U of penicillin/ml, and 50 μg of streptomycin/ml.

Generation of *Dnmt3L*$^{-/-}$ ESCs

Knockout was performed using TALEN technology. In brief, cells were transfected with the two TALEN constructs targeting Exon 1 of murine Dnmt3L and after 16 hr were seeded as a single cell. After 1 week, clones were picked and screened by western blotting. Positive clones were analyzed by genomic sequencing of the TALEN target.

For generation of a *Dnmt3L-ER-Dnmt3L*$^{-/-}$ stable ES clone, Dnmt3L KO cells were transduced with pBABE-Dnmt3L-ER retrovirus and were maintained under the selection with 1 μg/ml of puromycin for 7 days. Cells were treated with 1 μM of 4-OHT to induce nuclear localization of Dnmt3L-ER.

Generation of Mouse BirA-ES Cell Lines Stably Expressing Bio-Dnmt3L

To obtain Bio-Dnmt3L stable clone, BirA-ESCs (Driegen et al., 2005) were transfected with linearized Bio-Dnmt3L construct using Lipofectamine 2000 Transfection Reagent (Invitrogen) according to the manufacturer's protocol. Transfected cells were cultured for 10 days in growth medium with Blasticidin (Sigma), and drug-resistant clones were selected for Dnmt3L expression.

Figure 7. PRC2 Protein Ezh2 Recruits Dnmt3L on H3K27me3 Promoters

(A) Knockdown of Suz12 by shRNA led to an efficient downregulation of the Ezh2 protein and did not alter the level of the Dnmt3L protein, as demonstrated by immunoblotting analysis. β-actin was used as a loading control.

(B) Schematic representation of the *Rhox5* promoter region. Pd, distal promoter; Pp, proximal promoter. Lowercase letters show the position of the primers for the ChIP analysis.

(C and D) ChIP analysis of Ezh2 and Dnmt3L association with the *Rhox5* gene in Suz12 knockdown ESCs. Suz12 silencing resulted in a significant reduction in Ezh2 binding to the *Rhox5* promoter region as well as in Dnmt3L binding to this region. *$p < 0.01$. Data are represented as mean ± SD.

(E) Knockdown of Suz12 led to an efficient downregulation of the Ezh2 protein and did not alter the levels of the endogenous Dnmt3L or the Bio-Dnmt3L proteins, as demonstrated by immunoblotting analysis. β-actin was used as a loading control.

(F) Distribution of ChIP-seq Bio-Dnmt3L targets between intergenic (45%), promoter (3%), and gene body (52%) regions in ESCs.

(G) Normalized distribution of Bio-Dnmt3L-bound regions indicates that Bio-Dnmt3L is enriched on gene bodies and promoters on exons and repetitive sequences as microsatellites and LINE-SINE.

(H) Bio-Dnmt3L is enriched on bivalent and H3K27me3-only promoters with respect to the H3K4me3-only promoters.

(I) Gene ontology analysis revealed that Bio-Dnmt3L is enriched on the promoter of developmental-associated genes and on the body of cell-metabolism-associated genes.

(J) Heatmap representations of Ezh2, Suz12, and Bio-Dnmt3L distribution in control and Suz12 knockdown cells on TSS (±5 kb). The heatmap is rank ordered by H3K27me3. Bio-Dnmt3L correlates with PRC2 proteins Ezh2 and Suz12 in control cells, and this localization is reduced in shSuz12 cells.

(K) Plotting of the Bio-Dnmt3L ChIP-seq profile around TSS of H3K27me3-positive and -negative promoters confirms the reduction of signal following Suz12 knockdown.

(L) Genomic view of a representative PRC2 target region. Hoxa cluster is marked by H3K27me3 and Ezh2 in ESCs, and it shows an increase of 5mC after silencing of Dnmt3L. Bio-Dnmt3L signal is reduced after Suz12 knockdown.

See also Figure S7.

Nuclear Protein Extractions

Cells were harvested in PBS 1× and were resuspended in Isotonic Buffer (20mM HEPES [pH 7.5], 100 mM NaCl, 250 mM sucrose, 5 mM $MgCl_2$, and 5 μM $ZnCl_2$). Successively, cells were resuspended in isotonic buffer supplemented with 1% NP-40 to isolate the nuclei. The isolated nuclei were resuspended in digestion buffer (50 mM Tris-HCl [pH 8.0], 100 mM NaCl, 250 mM sucrose, 0.5 mM $MgCl_2$, 5 mM $CaCl_2$, and 5 μM $ZnCl_2$) and were treated with Micrococcal Nuclease at 30°C for 10 min.

Immunoprecipitation

Nuclear proteins from about 10 × 10^6 cells were incubated with 3 μg of specific antibody overnight at 4°C. Immunocomplexes were incubated with protein-G-conjugated magnetic beads (DYNAL, Invitrogen) for 2 hr at 4°C. Samples were washed four times with digestion buffer supplemented with 0.1% NP-40 at RT. Proteins were eluted by incubating with 0.4M NaCl TE buffer for 30 min and were analyzed by western blotting.

In Vitro Interaction Assay

The in vitro interaction assay was performed as previously described (Galvagni et al., 2001) (see Extended Experimental Procedures for details).

Microarray Analysis

Microarray analysis was performed on the Illumina Platform, and the results were analyzed using the BeadStudio Gene Expression Module (GX) (see Extended Experimental Procedures for details).

MeDIP-Seq and ChIP-Seq Analysis

MeDIP was performed using the MeDIP kit (55009, Active Motif), according to the manufacturer's protocol. The ChIP of Ezh2 was performed as previously described using 1% SDS buffer (Mikkelsen et al., 2007). ChIP of Bio-Dnmt3L and bioinformatics analyses are described in Extended Experimental Procedures.

Bisulfite Analysis

Bisulfite conversion was performed using EpiTect Bisulfite Kits (QIAGEN), and converted DNA was amplified using AccuPrime Taq DNA Polymerase (Invitrogen). The PCR product was cloned in TOPO-Blunt (using Zero Blunt TOPO PCR Cloning Kit, Invitrogen), and colonies were sequenced. Oligos for amplification were designed using Meth Primer Software (http://www.urogene.org/cgi-bin/methprimer/methprimer.cgi). Oligonucleotide sequences are in Table S5.

Chromatin Accessibility Assay

Chromatin accessibility was performed using EpiQ Chromatin Analysis Kit (from Biorad), according to the manufacturer's protocol. DNA was analyzed by quantitative real-time PCR by using a SYBR GreenER kit (Invitrogen).

Antibodies

The antibodies were purchased by Abcam (anti-Dnmt3l ab3493; anti-Dnmt3a; anti-Dnmt3b; anti-Nanog; anti-H3K9me3), by Immgenex (anti-Dnmt3a; anti-Dnmt3b; anti-Dnmt1, anti-*Rhox5*), by Cell Signaling (anti-Ezh2; anti-Suz12; anti-Rbbp4/7), by Millipore (anti-Sox2; anti-H3K27me3), by Sigma (anti-FLAG M2), by SantaCruz (anti-Oct3/4 sc-5279, anti-LaminA sc-20680), and by Neuromics (anti-Stella GT15240). Antibody anti-Dnmt3L was kindly provided by Dr. S. Yamanaka (Kyoto University, Japan).

ACCESSION NUMBERS

The ChIP-seq, MeDIP-seq, and expression microarray data sets have been deposited in Gene Expression Omnibus (GEO) under the accession number GSE44644.

SUPPLEMENTAL INFORMATION

Supplemental Information includes Extended Experimental Procedures, seven figures, and five tables and can be found with this article online at http://dx.doi.org/10.1016/j.cell.2013.08.056.

ACKNOWLEDGMENTS

This work was supported by the Associazione Italiana Ricerca sul Cancro (AIRC) and Regione Toscana programma salute. We thank Dr. S. Yamanaka (Kyoto University, Japan) for providing the anti-Dnmt3L antibody, Dr. En Li (Novartis, China) for providing the *Dnmt3a*$^{-/-}$ *Dnmt3b*$^{-/-}$ ESCs and Dr. Dies Meijer for providing the Avi-tag plasmid and BirA ESCs.

Received: March 12, 2013
Revised: July 19, 2013
Accepted: August 27, 2013
Published: September 26, 2013

REFERENCES

Bartke, T., Vermeulen, M., Xhemalce, B., Robson, S.C., Mann, M., and Kouzarides, T. (2010). Nucleosome-interacting proteins regulated by DNA and histone methylation. Cell *143*, 470–484.

Bestor, T.H. (2000). The DNA methyltransferases of mammals. Hum. Mol. Genet. *9*, 2395–2402.

Boch, J., Scholze, H., Schornack, S., Landgraf, A., Hahn, S., Kay, S., Lahaye, T., Nickstadt, A., and Bonas, U. (2009). Breaking the code of DNA binding specificity of TAL-type III effectors. Science *326*, 1509–1512.

Borgel, J., Guibert, S., Li, Y., Chiba, H., Schübeler, D., Sasaki, H., Forné, T., and Weber, M. (2010). Targets and dynamics of promoter DNA methylation during early mouse development. Nat. Genet. *42*, 1093–1100.

Bourc'his, D., and Bestor, T.H. (2004). Meiotic catastrophe and retrotransposon reactivation in male germ cells lacking Dnmt3L. Nature *431*, 96–99.

Bourc'his, D., Xu, G.L., Lin, C.S., Bollman, B., and Bestor, T.H. (2001). Dnmt3L and the establishment of maternal genomic imprints. Science *294*, 2536–2539.

Boyer, L.A., Plath, K., Zeitlinger, J., Brambrink, T., Medeiros, L.A., Lee, T.I., Levine, S.S., Wernig, M., Tajonar, A., Ray, M.K., et al. (2006). Polycomb complexes repress developmental regulators in murine embryonic stem cells. Nature *441*, 349–353.

Brinkman, A.B., Gu, H., Bartels, S.J.J., Zhang, Y., Matarese, F., Simmer, F., Marks, H., Bock, C., Gnirke, A., Meissner, A., and Stunnenberg, H.G. (2012). Sequential ChIP-bisulfite sequencing enables direct genome-scale investigation of chromatin and DNA methylation cross-talk. Genome Res. *22*, 1128–1138.

Chédin, F., Lieber, M.R., and Hsieh, C.-L. (2002). The DNA methyltransferase-like protein DNMT3L stimulates de novo methylation by Dnmt3a. Proc. Natl. Acad. Sci. USA *99*, 16916–16921.

Chen, Z.-X., Mann, J.R., Hsieh, C.-L., Riggs, A.D., and Chédin, F. (2005). Physical and functional interactions between the human DNMT3L protein and members of the de novo methyltransferase family. J. Cell. Biochem. *95*, 902–917.

Driegen, S., Ferreira, R., van Zon, A., Strouboulis, J., Jaegle, M., Grosveld, F., Philipsen, S., and Meijer, D. (2005). A generic tool for biotinylation of tagged proteins in transgenic mice. Transgenic Res. *14*, 477–482.

Ficz, G., Branco, M.R., Seisenberger, S., Santos, F., Krueger, F., Hore, T.A., Marques, C.J., Andrews, S., and Reik, W. (2011). Dynamic regulation of 5-hydroxymethylcytosine in mouse ES cells and during differentiation. Nature *473*, 398–402.

Fouse, S.D., Shen, Y., Pellegrini, M., Cole, S., Meissner, A., Van Neste, L., Jaenisch, R., and Fan, G. (2008). Promoter CpG methylation contributes to ES cell gene regulation in parallel with Oct4/Nanog, PcG complex, and histone H3 K4/K27 trimethylation. Cell Stem Cell *2*, 160–169.

Galvagni, F., Capo, S., and Oliviero, S. (2001). Sp1 and Sp3 physically interact and co-operate with GABP for the activation of the utrophin promoter. J. Mol. Biol. *306*, 985–996.

Gowher, H., Liebert, K., Hermann, A., Xu, G., and Jeltsch, A. (2005). Mechanism of stimulation of catalytic activity of Dnmt3A and Dnmt3B DNA-(cytosine-C5)-methyltransferases by Dnmt3L. J. Biol. Chem. *280*, 13341–13348.

Hata, K., Okano, M., Lei, H., and Li, E. (2002). Dnmt3L cooperates with the Dnmt3 family of de novo DNA methyltransferases to establish maternal imprints in mice. Development *129*, 1983–1993.

Hawkins, R.D., Hon, G.C., Lee, L.K., Ngo, Q., Lister, R., Pelizzola, M., Edsall, L.E., Kuan, S., Luu, Y., Klugman, S., et al. (2010). Distinct epigenomic landscapes of pluripotent and lineage-committed human cells. Cell Stem Cell *6*, 479–491.

Hayashi, K., Ohta, H., Kurimoto, K., Aramaki, S., and Saitou, M. (2011). Reconstitution of the mouse germ cell specification pathway in culture by pluripotent stem cells. Cell *146*, 519–532.

Jia, D., Jurkowska, R.Z., Zhang, X., Jeltsch, A., and Cheng, X. (2007). Structure of Dnmt3a bound to Dnmt3L suggests a model for de novo DNA methylation. Nature *449*, 248–251.

Jurkowska, R.Z., Rajavelu, A., Anspach, N., Urbanke, C., Jankevicius, G., Ragozin, S., Nellen, W., and Jeltsch, A. (2011a). Oligomerization and binding of the Dnmt3a DNA methyltransferase to parallel DNA molecules: heterochromatic localization and role of Dnmt3L. J. Biol. Chem. *286*, 24200–24207.

Jurkowska, R.Z., Jurkowski, T.P., and Jeltsch, A. (2011b). Structure and function of mammalian DNA methyltransferases. ChemBioChem *12*, 206–222.

Kaneda, M., Okano, M., Hata, K., Sado, T., Tsujimoto, N., Li, E., and Sasaki, H. (2004). Essential role for de novo DNA methyltransferase Dnmt3a in paternal and maternal imprinting. Nature *429*, 900–903.

Kareta, M.S., Botello, Z.M., Ennis, J.J., Chou, C., and Chédin, F. (2006). Reconstitution and mechanism of the stimulation of de novo methylation by human DNMT3L. J. Biol. Chem. *281*, 25893–25902.

Lee, T.I., Jenner, R.G., Boyer, L.A., Guenther, M.G., Levine, S.S., Kumar, R.M., Chevalier, B., Johnstone, S.E., Cole, M.F., Isono, K.-I., et al. (2006). Control of developmental regulators by Polycomb in human embryonic stem cells. Cell *125*, 301–313.

Li, E. (2002). Chromatin modification and epigenetic reprogramming in mammalian development. Nat. Rev. Genet. *3*, 662–673.

Li, Q., O'Malley, M.E., Bartlett, D.L., and Guo, Z.S. (2011). Homeobox gene Rhox5 is regulated by epigenetic mechanisms in cancer and stem cells and promotes cancer growth. Mol. Cancer *10*, 63.

Lienert, F., Wirbelauer, C., Som, I., Dean, A., Mohn, F., and Schübeler, D. (2011). Identification of genetic elements that autonomously determine DNA methylation states. Nat. Genet. *43*, 1091–1097.

Lindroth, A.M., Park, Y.J., McLean, C.M., Dokshin, G.A., Persson, J.M., Herman, H., Pasini, D., Miró, X., Donohoe, M.E., Lee, J.T., et al. (2008). Antagonism between DNA and H3K27 methylation at the imprinted Rasgrf1 locus. PLoS Genet. *4*, e1000145.

MacLean, J.A., 2nd, and Wilkinson, M.F. (2010). The Rhox genes. Reproduction *140*, 195–213.

Maclean, J.A., Bettegowda, A., Kim, B.J., Lou, C.H., Yang, S.M., Bhardwaj, A., Shanker, S., Hu, Z., Fan, Y., Eckardt, S., et al. (2011). The rhox homeobox gene cluster is imprinted and selectively targeted for regulation by histone h1 and DNA methylation. Mol. Cell. Biol. *31*, 1275–1287.

Margueron, R., and Reinberg, D. (2011). The Polycomb complex PRC2 and its mark in life. Nature *469*, 343–349.

Matarese, F., Carrillo-de Santa Pau, E., and Stunnenberg, H.G. (2011). 5-Hydroxymethylcytosine: a new kid on the epigenetic block? Mol. Syst. Biol. *7*, 562.

Meissner, A., Mikkelsen, T.S., Gu, H., Wernig, M., Hanna, J., Sivachenko, A., Zhang, X., Bernstein, B.E., Nusbaum, C., Jaffe, D.B., et al. (2008). Genome-scale DNA methylation maps of pluripotent and differentiated cells. Nature *454*, 766–770.

Mikkelsen, T.S., Ku, M., Jaffe, D.B., Issac, B., Lieberman, E., Giannoukos, G., Alvarez, P., Brockman, W., Kim, T.-K., Koche, R.P., et al. (2007). Genome-wide maps of chromatin state in pluripotent and lineage-committed cells. Nature *448*, 553–560.

Mohn, F., Weber, M., Rebhan, M., Roloff, T.C., Richter, J., Stadler, M.B., Bibel, M., and Schübeler, D. (2008). Lineage-specific polycomb targets and de novo DNA methylation define restriction and potential of neuronal progenitors. Mol. Cell *30*, 755–766.

Moscou, M.J., and Bogdanove, A.J. (2009). A simple cipher governs DNA recognition by TAL effectors. Science *326*, 1501–1501.

Neri, F., Zippo, A., Krepelova, A., Cherubini, A., Rocchigiani, M., and Oliviero, S. (2012). Myc regulates the transcription of the PRC2 gene to control the expression of developmental genes in embryonic stem cells. Mol. Cell. Biol. *32*, 840–851.

Ohm, J.E., McGarvey, K.M., Yu, X., Cheng, L., Schuebel, K.E., Cope, L., Mohammad, H.P., Chen, W., Daniel, V.C., Yu, W., et al. (2007). A stem cell-like chromatin pattern may predispose tumor suppressor genes to DNA hypermethylation and heritable silencing. Nat. Genet. *39*, 237–242.

Okano, M., Bell, D.W., Haber, D.A., and Li, E. (1999). DNA methyltransferases Dnmt3a and Dnmt3b are essential for de novo methylation and mammalian development. Cell *99*, 247–257.

Ooi, S.K.T., Qiu, C., Bernstein, E., Li, K., Jia, D., Yang, Z., Erdjument-Bromage, H., Tempst, P., Lin, S.-P., Allis, C.D., et al. (2007). DNMT3L connects unmethylated lysine 4 of histone H3 to de novo methylation of DNA. Nature *448*, 714–717.

Pasini, D., Bracken, A.P., Hansen, J.B., Capillo, M., and Helin, K. (2007). The polycomb group protein Suz12 is required for embryonic stem cell differentiation. Mol. Cell. Biol. *27*, 3769–3779.

Pastor, W.A., Pape, U.J., Huang, Y., Henderson, H.R., Lister, R., Ko, M., McLoughlin, E.M., Brudno, Y., Mahapatra, S., Kapranov, P., et al. (2011). Genome-wide mapping of 5-hydroxymethylcytosine in embryonic stem cells. Nature *473*, 394–397.

Pontier, D.B., and Gribnau, J. (2011). Xist regulation and function explored. Hum. Genet. *130*, 223–236.

Rush, M., Appanah, R., Lee, S., Lam, L.L., Goyal, P., and Lorincz, M.C. (2009). Targeting of EZH2 to a defined genomic site is sufficient for recruitment of Dnmt3a but not de novo DNA methylation. Epigenetics *4*, 404–414.

Schlesinger, Y., Straussman, R., Keshet, I., Farkash, S., Hecht, M., Zimmerman, J., Eden, E., Yakhini, Z., Ben-Shushan, E., Reubinoff, B.E., et al. (2007). Polycomb-mediated methylation on Lys27 of histone H3 pre-marks genes for de novo methylation in cancer. Nat. Genet. *39*, 232–236.

Schuettengruber, B., and Cavalli, G. (2009). Recruitment of polycomb group complexes and their role in the dynamic regulation of cell fate choice. Development *136*, 3531–3542.

Shen, X., Liu, Y., Hsu, Y.-J., Fujiwara, Y., Kim, J., Mao, X., Yuan, G.-C., and Orkin, S.H. (2008). EZH1 mediates methylation on histone H3 lysine 27 and complements EZH2 in maintaining stem cell identity and executing pluripotency. Mol. Cell *32*, 491–502.

Simmer, F., Brinkman, A.B., Assenov, Y., Matarese, F., Kaan, A., Sabatino, L., Villanueva, A., Huertas, D., Esteller, M., Lengauer, T., et al. (2012). Comparative genome-wide DNA methylation analysis of colorectal tumor and matched normal tissues. Epigenetics *7*, 1355–1367.

Stadler, M.B., Murr, R., Burger, L., Ivanek, R., Lienert, F., Schöler, A., van Nimwegen, E., Wirbelauer, C., Oakeley, E.J., Gaidatzis, D., et al. (2011). DNA-binding factors shape the mouse methylome at distal regulatory regions. Nature *480*, 490–495.

Suetake, I., Shinozaki, F., Miyagawa, J., Takeshima, H., and Tajima, S. (2004). DNMT3L stimulates the DNA methylation activity of Dnmt3a and Dnmt3b through a direct interaction. J. Biol. Chem. *279*, 27816–27823.

Turbendian, H.K., Gordillo, M., Tsai, S.-Y., Lu, J., Kang, G., Liu, T.-C., Tang, A., Liu, S., Fishman, G.I., and Evans, T. (2013). GATA factors efficiently direct cardiac fate from embryonic stem cells. Development *140*, 1639–1644.

Viré, E., Brenner, C., Deplus, R., Blanchon, L., Fraga, M., Didelot, C., Morey, L., Van Eynde, A., Bernard, D., Vanderwinden, J.-M., et al. (2006). The Polycomb group protein EZH2 directly controls DNA methylation. Nature *439*, 871–874.

Wei, W., Qing, T., Ye, X., Liu, H., Zhang, D., Yang, W., and Deng, H. (2008). Primordial germ cell specification from embryonic stem cells. PLoS ONE *3*, e4013.

West, J.A., Viswanathan, S.R., Yabuuchi, A., Cunniff, K., Takeuchi, A., Park, I.-H., Sero, J.E., Zhu, H., Perez-Atayde, A., Frazier, A.L., et al. (2009). A role for Lin28 in primordial germ-cell development and germ-cell malignancy. Nature *460*, 909–913.

Widschwendter, M., Fiegl, H., Egle, D., Mueller-Holzner, E., Spizzo, G., Marth, C., Weisenberger, D.J., Campan, M., Young, J., Jacobs, I., and Laird, P.W. (2007). Epigenetic stem cell signature in cancer. Nat. Genet. *39*, 157–158.

Wu, H., Coskun, V., Tao, J., Xie, W., Ge, W., Yoshikawa, K., Li, E., Zhang, Y., and Sun, Y.E. (2010). Dnmt3a-dependent nonpromoter DNA methylation facilitates transcription of neurogenic genes. Science *329*, 444–448.

Zhang, Y., Jurkowska, R., Soeroes, S., Rajavelu, A., Dhayalan, A., Bock, I., Rathert, P., Brandt, O., Reinhardt, R., Fischle, W., and Jeltsch, A. (2010). Chromatin methylation activity of Dnmt3a and Dnmt3a/3L is guided by interaction of the ADD domain with the histone H3 tail. Nucleic Acids Res. *38*, 4246–4253.

EXTENDED EXPERIMENTAL PROCEDURES

MeDIP-Seq and ChIP-Seq Analysis

MeDIP was performed using the MeDIP kit (55009, Active Motif), according to the manufacturer's protocol. The ChIP of Ezh2 was performed as previously described using 1% SDS buffer (Mikkelsen et al., 2007). For ChIP of Bio-Dnmt3L, approximately $2x10^7$ cells were cross-linked by addition of formaldehyde to 1% for 10 min at RT, quenched with 0.125 M glycine for 5 min at RT, and then washed twice in 1x PBS. The cells were resuspended in Isotonic buffer supplemented with 1% NP-40 to isolate nuclei. The isolated nuclei were then resuspended in ChIP Buffer (20 mM Tris-HCl pH 8.0, 150 mM NaCl, 2 mM EDTA, 1% Triton X-100, 0.15% SDS and protease inhibitors). Extracts were sonicated using the Bioruptor® Twin (Diagenode) for 2 runs of 10 cycles [30 s "ON," 30 s "OFF"] at high power setting. Cell lysate was centrifuged at 12,000 g for 10 min at 4°C. Streptavidin beads (Dynabeads® MyOneTM Streptavidin T1) were saturated with PBS/1% BSA at RT for 1 hr, and then incubated with sample at 4°C for 4 hr on a rotator. Immunoprecipitated complexes were successively washed with Washing Buffer I (2% SDS), Washing Buffer II (50 mM HEPES pH 7.5, 500 mM NaCl, 0.1% Deoxycholate, 1% Triton X-100, 1 mM EDTA), Washing Buffer III (10 mM Tris-Cl pH 8.1, 250 mM LiCl, 0.5% NP-40, 0.5% Deoxycholate, 1 mM EDTA,) and TE buffer (10 mM Tris-HCl pH 7.5, 1 mM EDTA). All washes were performed at RT for 8 min on a rotator. SDS Elution Buffer (50 mM Tris-HCl pH 8.0, 10 mM EDTA, 1% SDS) was added and incubated at 65°C overnight to reverse crosslink protein-DNA complexes. After decrosslinking, DNA was purified using QIAQuick PCR Purification Kit (QIAGEN) according to the manufacturer's instructions.

Sequencing was performed on the Illumina HiScanSQ Platform. Reads were mapped to the mouse genome (mm9 assembly) using Bowtie version 0.12.7, reporting only unique hits with up to two mismatches. Redundant reads were collapsed, and peak calling was performed using MACS version 1.4.1. For comparative analysis, we downloaded GEO Data sets data for ESC histone modifications (GSE12241 and GSE11172), MeDIP (GSE31343, GSE28682 and Sequence Read Archive ERP000570), MethylCap (GSE31343), transcription factors (GSE11431) and Bisulfite-seq (GSE30206). Data mapped on mouse mm8 assembly were transposed to mm9 assembly using a liftover tool. Heatmap and comparative analysis were performed using custom Perl scripts. Motif discovery was performed using Homer v4.2 (Heinz et al., 2010). The significance of ChIP-seq data sets overlapping was given by Z-Scores.

Generation of a Tetracycline-Inducible 293 Stable Cell Line

A tetracycline-inducible HEK293 cell line that stably expressed FLAG-Dnmt3L was generated by using the Invitrogen's Flp-T-Rex System. The FLAG-pcDNA5/FRT/TO expression vector containing the gene of interest was inserted into the cells via Flp recombinase-mediated DNA recombination at the FRT site. The transfected cells were selected on the basis of hygromycin B (Sigma) resistance, and pool clones were isolated.

Clones were cultivated in DMEM high glucose medium (Invitrogen) supplemented with 10% FBS (Sigma), 1mM sodium pyruvate (Invitrogen), 50 U of penicillin/ml, 50 μg of streptomycin/ml, and 100 μg/ml hygromycin (Invitrogen) for 2/3 weeks.

Transfection and Transduction

For silencing, ES cells were transfected as previously described in (Neri et al., 2012) and were maintained under the selection with 1 μg/ml of Puromycin for 3 days prior to perform experiments in ESCs.

Virus particles for transduction were prepared according to the manufacturer's instructions (Retro-X HTX Packaging System, Clontech).

HEK293 T-Rex cell lines were transfected using Attractene Transfection Reagent (QIAGEN) according to the manufacturer's protocol.

For overexpression experiments, E14 mouse ES cells were transfected using Lipofectamine 2000 Transfection Reagent (Invitrogen) according to the manufacturer's protocol. Transfected cells were harvested 24 hr after transfection.

DNA Constructs and Recombinant Proteins

Murine Dnmt3L cDNA construct was purchased from Addgene (plasmid 13356) and cloned into FLAG-pcDNA5/FRT/TO vector using the EcoRI and *XhoI* restriction sites. The deletion mutants Dnmt3L ΔPHD (aa 1-120;199-421) and Dnmt3l ΔC (aa 1-206) were generated by PCR amplification of the corresponding fragments and cloned into FLAG-pcDNA5/FRT/TO expression vector using the *EcorI* and *XhoI* restriction sites. Biotag-Dnmt3L construct was generated by PCR amplification of the Biotag-Dnmt3L fragment and cloned into pEF6/V5-His TOPO expression vector.

To generate the Dnmt3L-ER construct, Dnmt3L was subcloned into the pBABE-ER expression vector using the BglII and EcoRI restriction sites. *Rhox5* FL cDNA (cDNA-*Rhox5* pSPORT1) was purchased by Open Biosystem and cloned into pcDNA5/FRT/TO using the KpnI and *Not*I restriction sites.

The shRNA constructs were purchased from Open Biosystems for Dnmt3L (TRCN0000039104, TRCN0000039106, TRCN0000039108), *Rhox5* (TRCN0000086148, TRCN0000086151), *Rhox6* (TRCN0000070736, TRCN0000070737), *Rhox9* (TRCN0000070408, TRCN0000070409), and Suz12 (TRCN0000123889). Talen vectors targeting Exon 1 of murine Dnmt3L were purchased from ZGeneBio. Recombinant GST-Ezh2 was purchased from Abnova (Cat. No. H00002146-P01). Control siRNA (AllStars negative Control siRNA) was purchased from QIAGEN. siRNA targeting Dnmt3L (UGAAUCACCAUAAGAUGA) and targeting *Rhox5* (1: AGCCAUCUCCCUGCACAG, 2: CUCACCUCCUGCCUUCCG) were purchased from Eurofins MWG Operon.

Immunodepletion

Each round of immunodepletion was performed by incubating the nuclear extract with 2 μg of specific antibody for 2 hr at 4°C on a rotator and, then, with Protein G-conjugated magnetic beads (DYNAL, Invitrogen) for 2 hr at 4°C on a rotator. In total, four rounds of immunodepletion were performed.

Purification of FLAG-Dnmt3L

Recombinant FLAG-Dnmt3L protein was produced and purified from the tetracycline-inducible 293 cell line, which stably expresses FLAG-Dnmt3L, using anti-FLAG M2 affinity gel (Sigma). The isolated complexes were eluted with 3xFLAG peptide (Sigma) for 1 hr at 4°C on a rotator and, then, were additionally purified on a Superdex 200 column (GE Healthcare, Life Sciences), to isolate free FLAG-Dnmt3L.

In Vitro Interaction Assay

The in vitro interaction assay was performed as previously described (Galvagni et al., 2001), by incubating recombinant GST-Ezh2 or GST with FLAG peptide or FLAG-Dnmt3L magnetic beads in Interaction buffer (50mM Tris-HCl pH 8.0, 100mM NaCl, 10% glycerol, 0.5mM $MgCl_2$, 5 μM $ZnCl_2$) for 2 hr at 4°C on a rotator. After four washes with the same buffer, the interacting proteins were eluted with 0.4M NaCl TE buffer for 30 min and were analyzed by western blotting.

DNA Methyltransferase Activity Assay

Quantification of DNA Methyltransferase activity was performed using the EpiQuik DNA Methyltransferase Activity/Inhibition Assay Kit (Epigentek).

Gel Filtration Chromatography

Gel filtration chromatography was performed on a Superose-6 10/300 GL column (GE Healthcare) using an AKTA purifier system (GE Healthcare). Nuclear extract from about $60x10^6$ cells was loaded onto the column and separated in gel filtration buffer (50 mM Tris-HCl pH 8.0, 100 mM NaCl, 250 mM sucrose, 0.5 mM $MgCl_2$, 5 mM $CaCl_2$, 5 μM $ZnCl_2$) at a flow rate of 0.3 ml/min and 0.5-ml fractions were collected. The molecular mass standards (GE Healthcare) used to calibrate the column were blue dextran (2000 kDa), thyroglobulin (669 kDa), ferritin (440 kDa), catalase (240 kDa) and aldolase (158 kDa). The void volume was between 8 and 8.5 ml (corresponding to the fractions 3 and 4). The fractions 2 to 22 were immunoprecipitated with anti-Dnmt3L antibody and analyzed by western blotting.

Chromatin Immunoprecipitation

Each ChIP experiment was performed on at least three independent biological samples and was performed as previously described (Zippo et al., 2009). DNA was analyzed by quantitative real-time PCR by using a SYBR GreenER kit (Invitrogen). All of the experimental values were normalized to those obtained with a nonimmune serum, and the values were divided by the input. The data shown represent triplicate real-time quantitative PCR measurements of the immunoprecipitated DNA. The data are expressed as (%) 1/100 of the DNA inputs. Error bars represent standard deviations that were determined from triplicate experiments. Oligonucleotide sequences are in Table S4.

RNA Analysis

RNA samples were extracted directly from cultured cells using the Trizol reagent (GIBCO) followed by isopropanol precipitation. RNA was analyzed by quantitative real-time PCR by using a Superscript III platinum Onestep qRT-PCR System kit (Invitrogen). Error bars represent standard deviations determined from triplicate experiments. Oligonucleotide sequences are in Table S3. For RT-PCR analysis of the pd and the pp *Rhox5* transcripts, primers were designed on exons 2 and 3 for the pd transcript and on exon 3 (in the 5′UTR region not corresponding to the pd transcript) for the pp transcript.

FACS Analysis

Cultured cells were harvested after incubation with dissociation buffer (GIBCO) under gentle agitation and were incubated for 30 min in phosphate-buffered saline (PBS)-5% FBS on ice, to block nonspecific binding. Cells were then incubated with primary antibodies for 30 min in PBS-1% bovine serum albumin (BSA) and, after 3 washes, were stained with conjugated secondary antibodies. Cells were analyzed by a fluorescence-activated cell scan (FACS).

Immunostaining

Cells were plated on coated cover glasses; they were fixed with 4% paraformaldehyde in PBS for 20 min at room temperature (RT); they were washed twice and were incubated with the blocking buffer (PBS + 1% BSA + 0.1% Triton X-100). The fixed cells were incubated with primary antibody in blocking buffer for 1 hr at RT followed by 3 washes and incubation with conjugated secondary antibodies in blocking buffer for 1 hr at RT.

Microarray Analysis

Microarray analysis was performed on the Illumina Platform and the results were analyzed using the BeadStudio Gene Expression Module (GX). To exclude shRNA off-targets, we considered only genes that were regulated by at least two different shRNAs; the fidelity and efficiency of the three knockdowns was validated by applying the Pearson correlation, which shows high similarity. Data were background adjusted and quartile normalized using default parameters in the Genome BeadStudio Software. Probes with Log2 $|FC| > 1$ and p value < 0.05 were selected for downstream analysis. Heatmap plots were performed through the Bioconductor package in R. Differential expression analysis of the upregulated or downregulated genes was performed by plotting genes with their Log2 expression value using Excel. Microarray data from Literature were obtained from Gene Expression Omnibus (GEO Data set: GSE7948, GSE43831, GSE12982). Upregulated or downregulated genes in Dnmt3L knockdown ES cells are shown in Table S1 and Table S2.

SUPPLEMENTAL REFERENCES

Heinz, S., Benner, C., Spann, N., Bertolino, E., Lin, Y.C., Laslo, P., Cheng, J.X., Murre, C., Singh, H., and Glass, C.K. (2010). Simple combinations of lineage-determining transcription factors prime cis-regulatory elements required for macrophage and B cell identities. Mol. Cell *38*, 576–589.

Zippo, A., Serafini, R., Rocchigiani, M., Pennacchini, S., Krepelova, A., and Oliviero, S. (2009). Histone crosstalk between H3S10ph and H4K16ac generates a histone code that mediates transcription elongation. Cell *138*, 1122–1136.

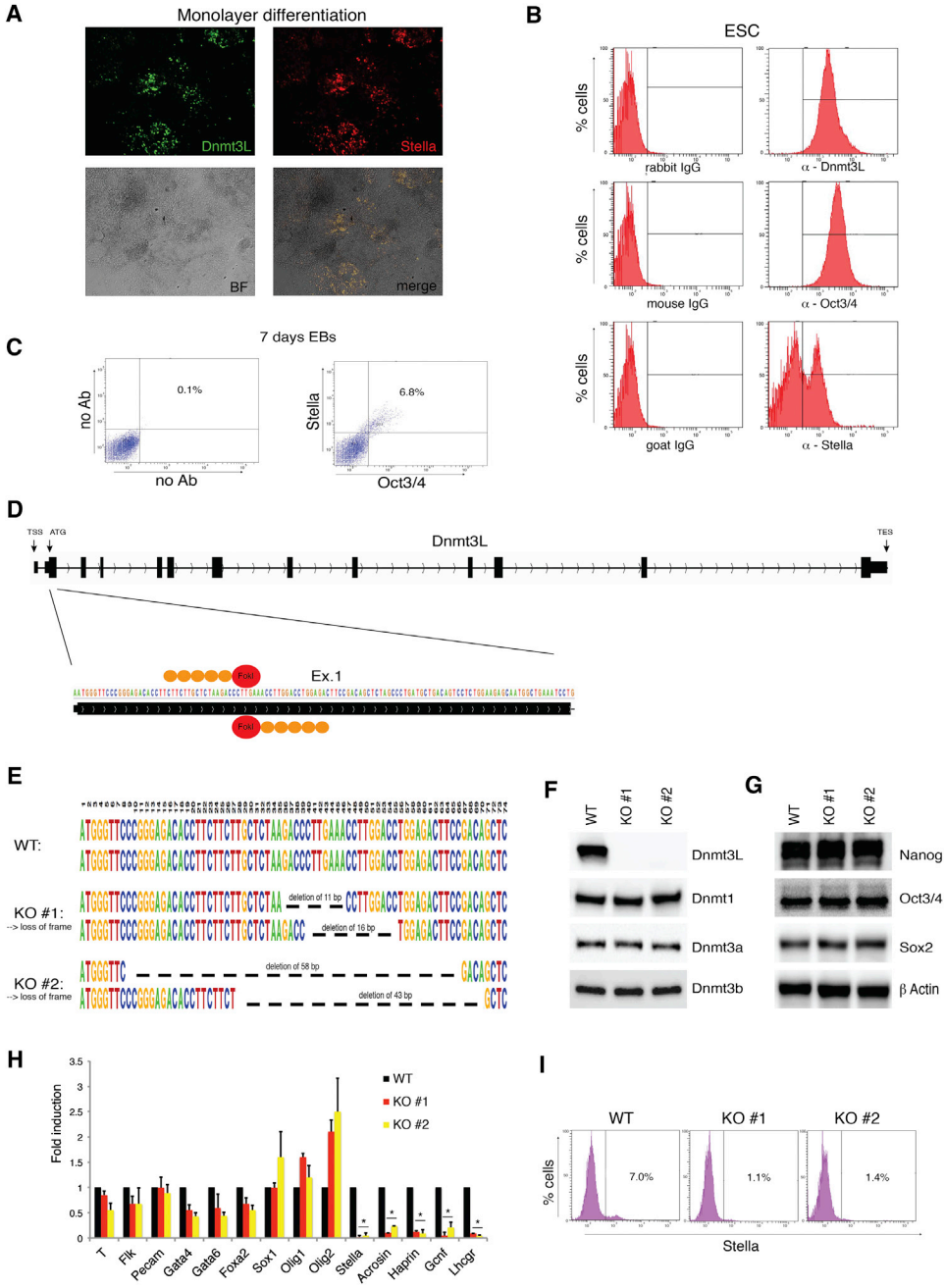

Figure S1. Dnmt3L Is a Marker of Primordial Germinal Cells, Related to Figure 1

(A) Immunofluorescence analysis shows the coexpression of Stella together with Dnmt3L in ESCs differentiated by a monolayer differentiation method.

(B and C) Specificity of the antibodies used in FACS analyses.

(D) Scheme of Dnmt3L gene and TALEN target site used in this study.

(E) TALEN caused biallelic deletion of part of the first exon of Dnmt3L in ESCs, leading to loss of frame.

(F and G) Knockout of Dnmt3L did not alter the expression of the other Dnmts and of the pluripotency-related genes, such as Nanog, Oct3/4, and Sox2. The protein levels were measured by western blot analysis. β−Actin was used as a loading control.

(H) Dnmt3L$^{-/-}$ cells show a reduction of PGC markers during differentiation as shown by RT-qPCR analysis of EBs at seven days. The data are represented as mean ± SD.

(I) FACS analysis demonstrates that Dnmt3L$^{-/-}$ do not forms Stella positive cells.

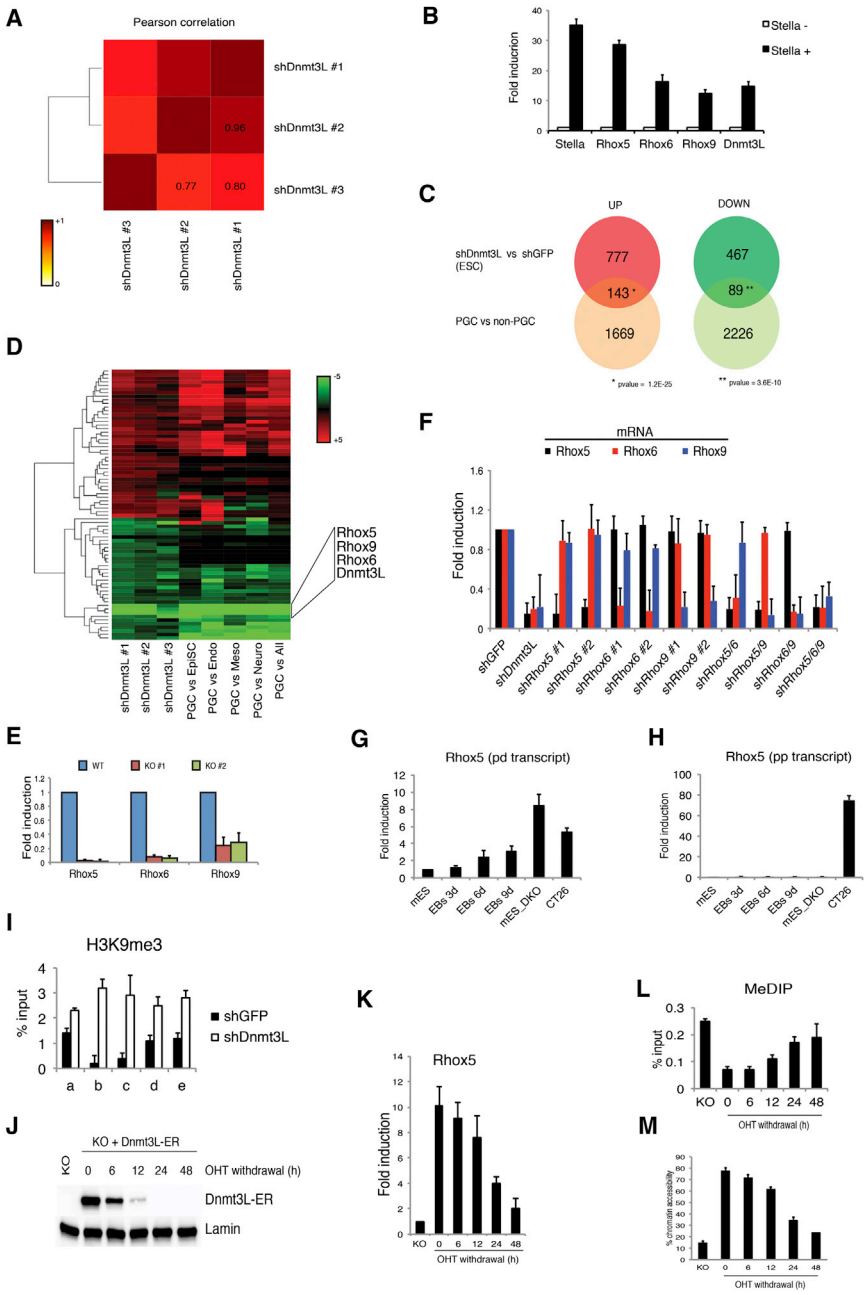

Figure S2. Dnmt3L Modulates the Expression of PGCs' Specific Genes, Related to Figure 2

(A) Correlation analysis of the three different Dnmt3L knockdowns used in microarray analysis of the misregulated genes (Pearson correlation R $\geq$ 0.77).

(B) Validation of West et al. microarray data by RT-qPCR analysis demonstrating that Dnmt3L and *Rhox* genes are upregulated together in Stella positive cells at 7 days EBs. The data are represented as mean ± SD.

(C) A comparison of the genes that are regulated upon Dnmt3L knockdown in ESC against the genes that are differentially expressed in PGCs versus the average of the other differentiating layers.

(D) Clustering analysis of the shared genes shown in Figure 2A of microarray data of PGC versus other differentiation stages. This analysis confirms the clustering between Dnmt3L and the *Rhox5*, *Rhox6* and *Rhox9* genes.

(E) The downregulation of the three *Rhox* genes *Dnmt3L*$^{-/-}$ was measured by RT-qPCR analysis (*p value < 0.001). The data are represented as mean ± SD.

(F) The efficiency of the *Rhox5*, *Rhox6* and *Rhox9* knockdowns using various shRNAs in ESC was evaluated by RT-PCR analysis. The data are represented as mean ± SD.

(G and H) RT-PCR analysis of the *Rhox5* proximal or distal promoter transcripts in ESCs, differentiated ESCs, and Dnmt3a/3b DKO ESCs. CT26 mouse colon cancer cells were used as a positive control for the proximal promoter transcript. The data are represented as mean ± SD.

(legend continued on next page)

(I) ChIP analysis demonstrates an increase of H3K9me3 heterochromatin mark upon Dnmt3L knockdown within the shown *Rhox5* regions. The data are represented as mean ± SD.

(J) The nuclear exit timing of the DnmtL-ER fusion protein after OHT withdrawal. The nuclear extracts obtained from the time course analysis of *Dnmt3L*$^{-/-}$-Dnmt3L-ER cells were analyzed by western blotting. Lamin was used as a loading control.

(K) RT-PCR analysis demonstrates that the *Rhox5* expression increases in *Dnmt3L*$^{-/-}$ cells expressing the exogenous activated Dnmt3L-ER fusion protein and that it decreases following OHT withdrawal. The data are represented as mean ± SD.

(L) MeDIP analysis of the *Rhox5* promoter on the probe "c" (as shown in Figure 3A) shows a decrease in DNA methylation in *Dnmt3L*$^{-/-}$ cells expressing the exogenous activated Dnmt3L-ER and an increase following OHT withdrawal. The data are represented as mean ± SD.

(M) An increase of chromatin accessibility of *Rhox5* promoter on probe "c" (as shown in Figure 3A) is observed in Dnmt3L$^{-/-}$ cells expressing the exogenous activated Dnmt3L-ER respect to the Dnmt3L$^{-/-}$ cells. A decrease of chromatin accessibility is observed after OHT withdrawal. The data are represented as mean ± SD.

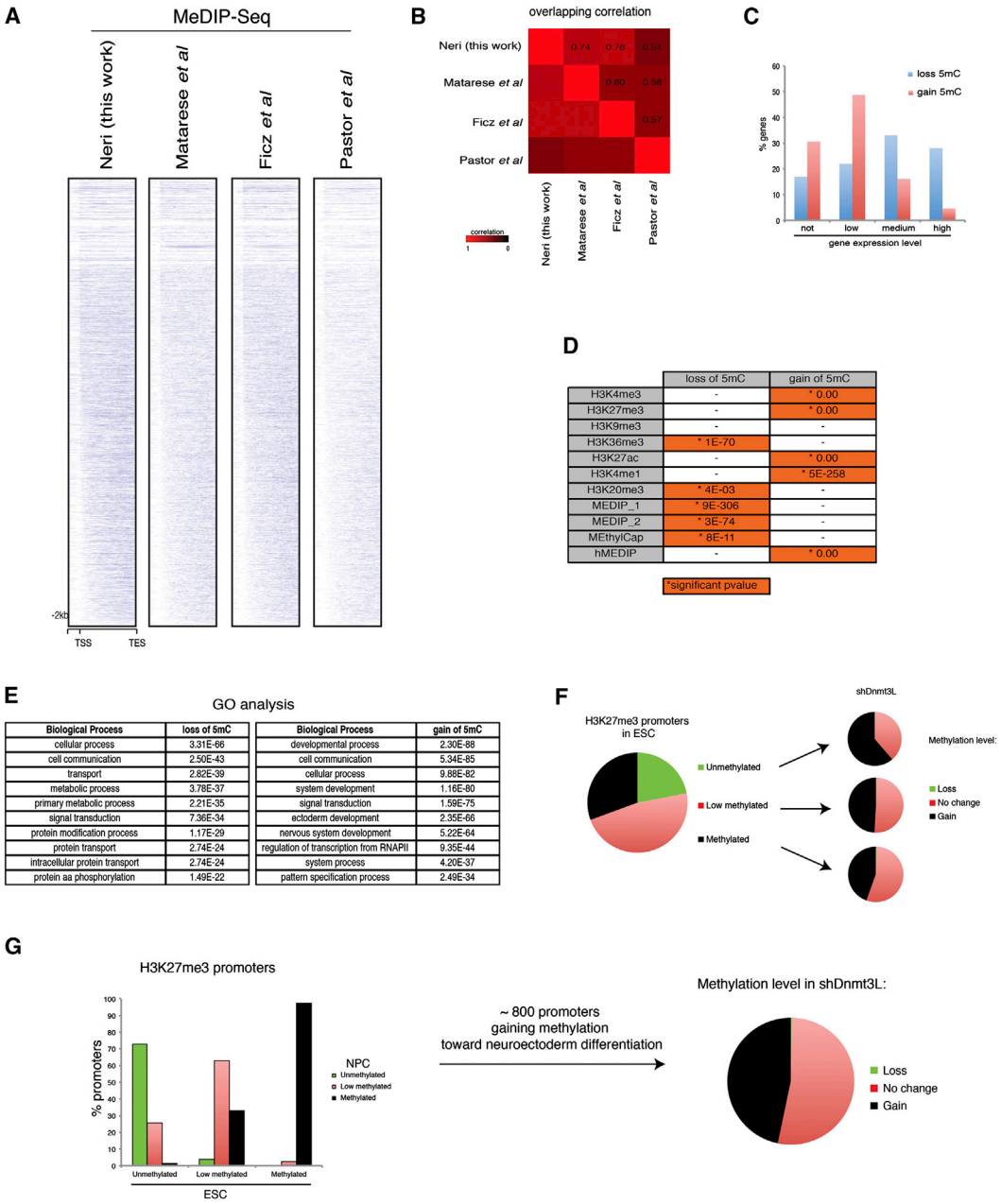

Figure S3. The Double Role of Dnmt3L in 5mC Regulation, Related to Figure 4

(A and B) Heatmap representations of MeDIP-seq analyses performed in this work and by others, and the overlapping correlation between them.

(C) The percentage of genes that became DNA methylated upon Dnmt3L knockdown shows an enrichment in genes that are not expressed or expressed at low level while the percentage of genes with a decrease in DNA methylation upon Dnmt3L knockdown shows an enrichment in genes that are expressed at medium or high level.

(D) Significant enrichments in genomic overlappings between DNA and histone modification with differentially methylated regions (DMR) between control or Dnmt3L knockdown cells.

(E) Gene ontology analysis of genes that show differentially methylated regions.

(F) Gain of methylation occurs in all H3K27me3-positive promoters independently from the initial methylation state of the promoter. H3K27me3 promoters have been classified in unmethylated, low methylated, and methylated as defined in (Stadler et al., 2011).

(G) H3K27me3 promoters tend to became more methylated during differentiation in NPC and very few show a loss of methylation (Stadler et al., 2011). About half of the H3K27me3-positive promoters that gain DNA methylation are hypermethylated in Dnmt3L silenced ESCs.

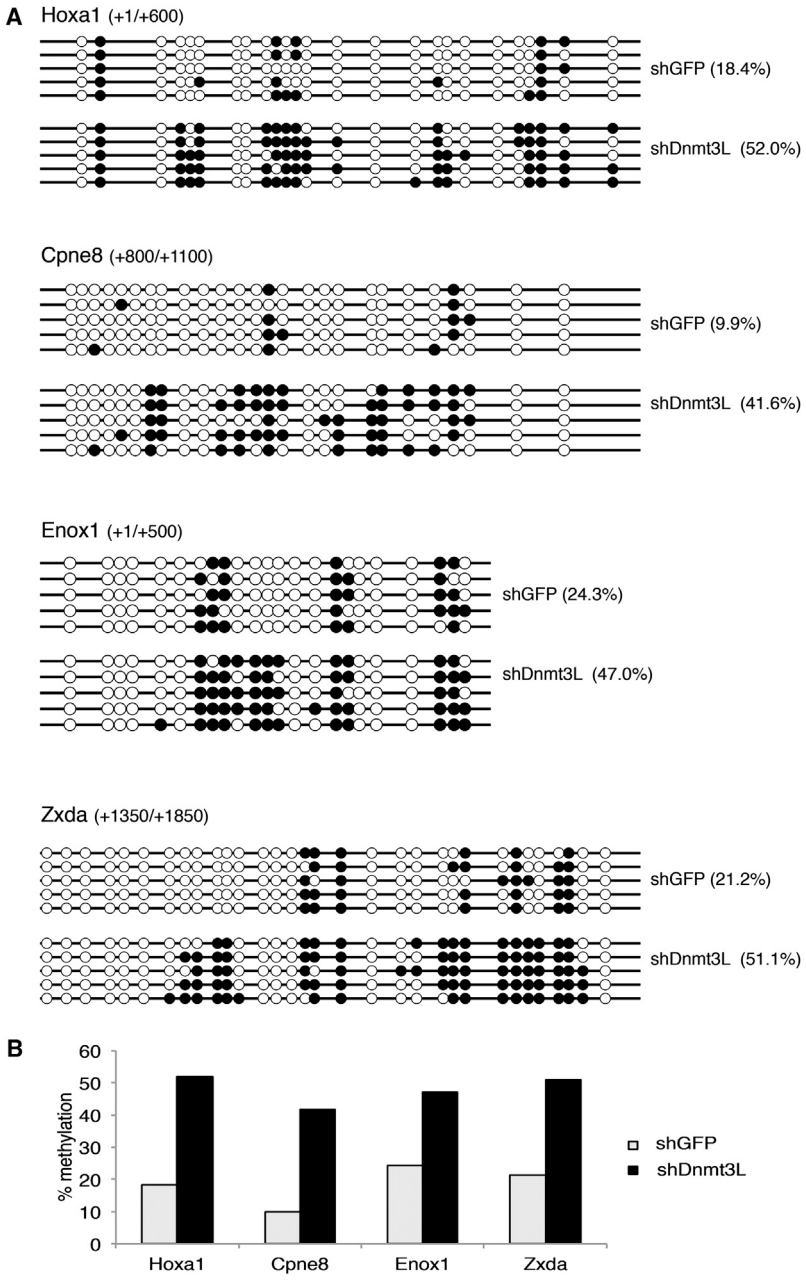

Figure S4. Dnmt3L Maintains Developmental Genes in the Hypomethylated State, Related to Figure 4

(A and B) Bisulfite-sequencing analysis of the indicated genes in control and Dnmt3L knockdown cells, and its quantification shown as apercentage DNA methylation.

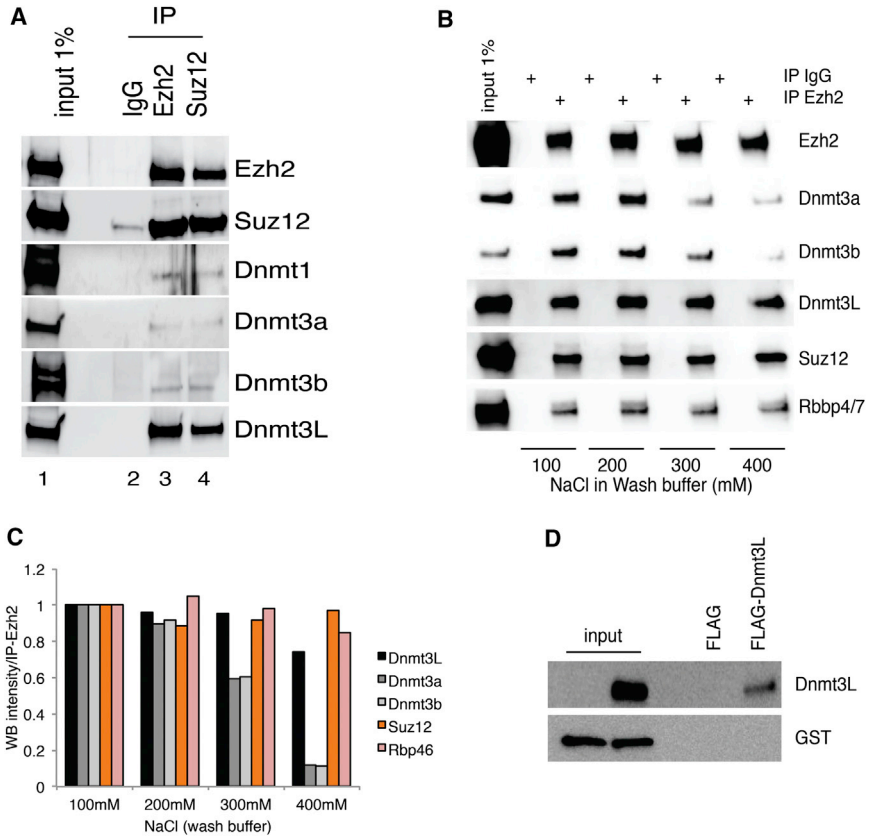

Figure S5. Dnmt3L Interacts with PRC2 in ESCs, Related to Figure 5

(A) Endogenous PRC2 proteins Ezh2 and Suz12 coimmunoprecipitate with Dntm3L in ESCs as shown by immunoprecipitation. 1% of the nuclear extract was loaded as an input.

(B) Endogenous Ezh2-Dnmt3L interaction is less susceptible to high salt concentrations than Ezh2-Dnmt3a/3b interaction. 1% of the nuclear extract was loaded as an input.

(C) Quantification of the bands of the western blotting of Figure S5B. The values are normalized on Ezh2 immunoblot and on the first condition (100mM of NaCl).

(D) GST does not interact with the FLAG-Dnmt3L recombinant protein.

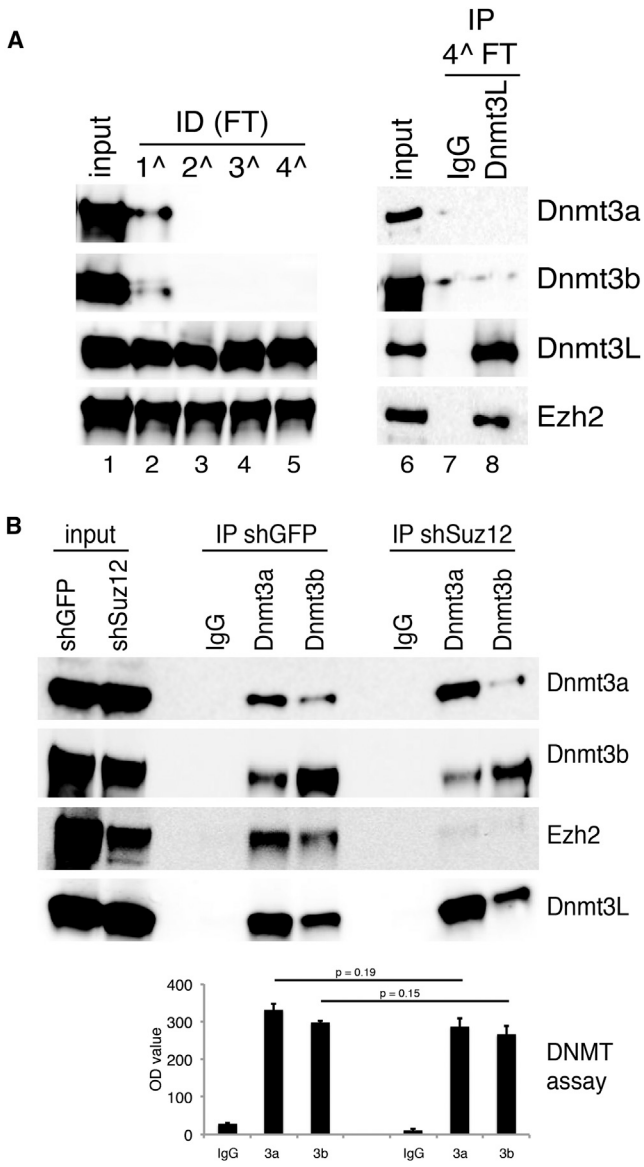

Figure S6. Dnmt3L Forms a Dnmt3a/b-Independent Complex with PRC2, Related to Figure 6

(A) Immunodepletion of the endogenous Dnmt3a and Dnmt3b proteins in ESCs. Four rounds of immunodepletion were performed using antibodies against Dnmt3a and Dnmt3b. The final flow-through was subsequently immunoprecipitated by anti-Dnmt3L antibody and the interacting proteins were analyzed by immunoblotting using the indicate antibodies.

(B) No significant changes in DNA methylation activity of the Dnmt3a/3b immunoprecipitated complexes were found between control shGFP and shSuz12 cells. The data are represented as mean ± SD.

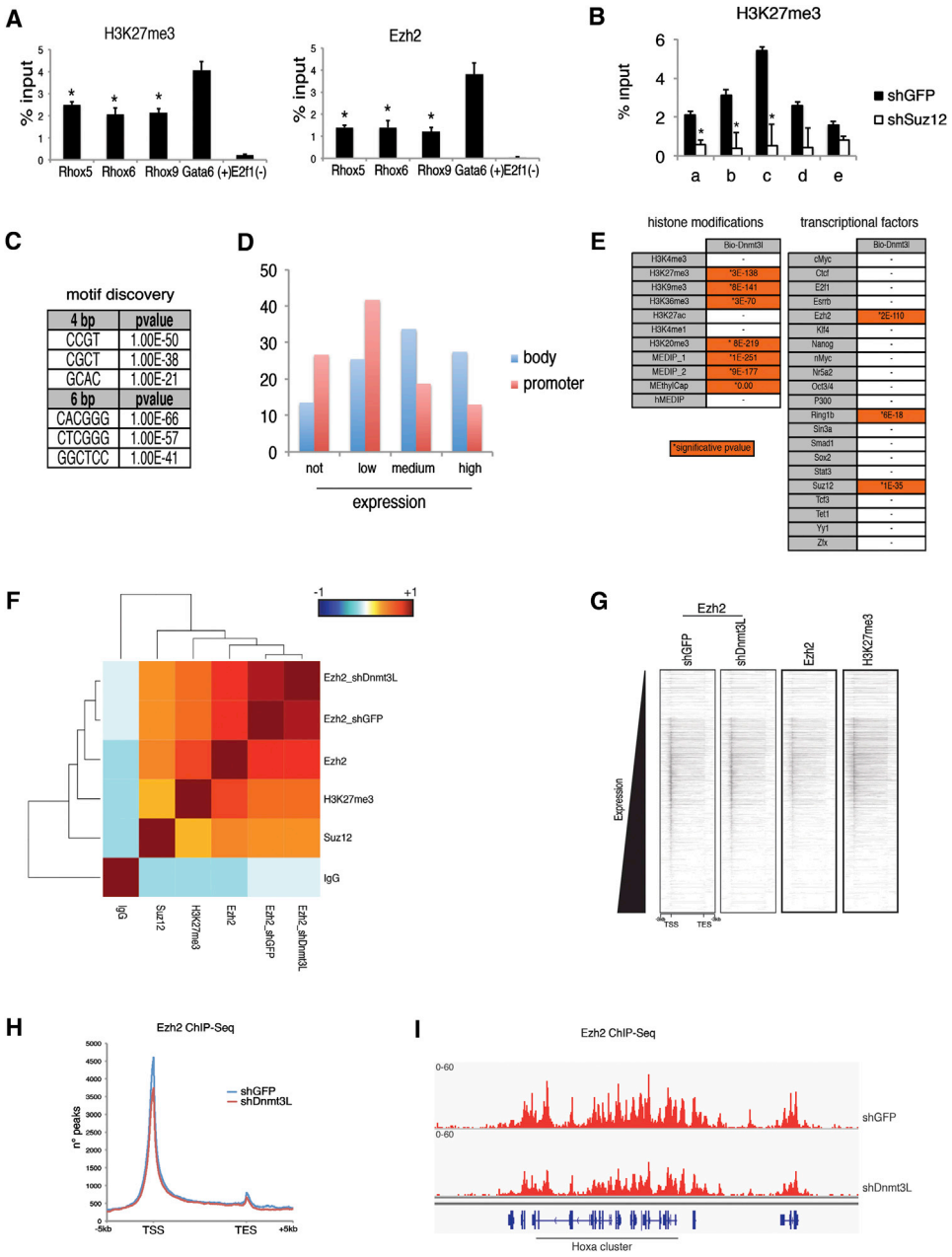

Figure S7. PRC2 Protein Ezh2 Recruits Dnmt3L on Developmental Genes, Related to Figure 7

(A) The *Rhox* genes are marked by H3K27me3 modification and bound by the Ezh2 protein in ESCs as shown by ChIP-analysis. The Gata6 gene was used as a positive control, the E2f1 gene was used as a negative control. (*p value < 0.001) The data are represented as mean ± SD.

(B) Knockdown of Ezh2 leads to a reduction of H3K27me3 within the shown regions of the *Rhox5* gene as shown by ChIP-analysis. (*p value < 0.01) The data are represented as mean ± SD.

(C) Motif discovery of the regions enriched in Bio-Dnmt3L ChIP-seq shows a significant enrichment of the CG dinucleotide.

(D) Bio-Dnmt3L is enriched on the promoters of not and low expressed genes and on the bodies of the medium and high expressed genes.

(E) Bio-Dnmt3L is enriched on H3K27me3, H3K9me3, H3K36me3, H3K20me3 and 5mC marked genomic regions and correlates with the PRC2 protein Ezh2.

(F) Clustering analysis of the global Pearson correlation of the Ezh2 ChIP-seq used in this study with the other available in literature, shows the bona fide of our analysis.

(G) Heatmap representations of Ezh2 ChIP-seq in shGFP and shDnmt3L cells show no change in global Ezh2 distributions.

(H and I) Ezh2 ChIP-seq profiles on average gene or on Hoxa clusters shows a minor signal intensity in shDnmt3L cells respect to control shGFP cells, but no changes in Ezh2 localization.